Interaction Notes
Note 379
September 1979

CALCULATION OF THE SINGULARITY EXPANSION METHOD PARAMETERS FROM THE TRANSIENT RESPONSE OF A THIN WIRE

K. S. Cho
J. T. Cordaro

The University of New Mexico
Albuquerque, New Mexico 87131

ABSTRACT

The problem of determining the singularity expansion method (SEM) parameters from transient thin-wire data is examined. A computer code is used to generate response data. The SEM parameters are computed from these data. For noisy data, it is shown that the parameter values can be improved by signal averaging.

ACKNOWLEDGEMENT

The authors express their appreciation to Carl E. Baum of the Air Force Weapons Laboratory for several helpful discussions on SEM. This work was sponsored by the USAF under Grant No. AFOSR-78-3723.

TABLE OF CONTENTS

TABLE OF CONTENTS (continued)

LIST OF FIGURES

LIST OF FIGURES (continued)

LIST OF FIGURES (continued)

CHAPTER I

INTRODUCTION

The singularity expansion method (SEM) [1] has proven to be a useful tool for the analysis of electromagnetic scattering problems. The SEM gives a relation between the incident field and the induced currents and charges on a body. In this relation, the natural response is expressed as a sum of complex exponentials. The SEM parameters in the sum (natural frequencies, natural modes, and coupling coefficients) together with the incident waveform describe the scattering problem in a useful and compact way.

A number of investigators have analyzed simple bodies using SEM. In the original SEM paper, Baum [2] treated a perfectly conducting sphere in free space. He obtained analytical expressions for surface current density and surface charge density. The SEM parameters were found numerically from these expressions. Tesche [3] applied the method of moments to Pocklington's equation and computed the SEM parameters for a thin wire in free space. Wilton and Umashankar [4] analyzed an L-shaped wire. Marin [5] derived approximate expressions for the natural frequencies and natural modes of several thin-wire structures. Marin and Liu [6] used some of these results to suggest a simple way of solving transient thin-wire problems.

All the work mentioned so far is theoretical in the sense that the SEM parameters were found by solving equations relating the incident field and the corresponding body response. For people involved in electromagnetic pulse (EMP) testing, it is of interest to know whether the SEM parameters can be computed from measured test data.

Van Blaricum and Mittra [7] began work in this area. They used Prony's method [8] to compute the natural frequencies of computer-generated transient data. Their results gave impetus to a number of other studies. Lager, Hudson, and Poggio [9] applied Prony's method to several test cases and provided some guidelines for applying the method [10]. There are some problems involved in using Prony's method on noisy data [11]. The performance of the method can be improved by using an iterative technique. Such a scheme has been applied successfully to actual EMP test data [12]. At this point the problem of how to compute the natural frequencies of a body from transient data appears to be fairly well understood.

The next line of work involves developing techniques for computing the other two parameters (natural modes and coupling coefficients) from real data. Pearson and Robertson [13] showed that the natural modes for a thin wire can be computed from transient data. They generated current responses using a thin-wire computer code. The exciting function was a Gaussian voltage pulse applied across a gap in the wire. They were able to compute

natural frequencies and natural modes that agree well with those found by Tesche [3].

The work reported here is a continuation of the efforts mentioned above. The aim is to develop techniques for estimating the SEM parameters from real test data. A general approach for estimating the parameters consists of measuring current waveforms at a number of different locations on a test body for various angles of incidence and polarization. The parameters are estimated from these current waveforms. At present, there are not enough appropriate test data to use in the calculations. As an alternative, the same thin-wire computer code adopted in several of the references was used to generate transient current data. The thin wire is a simple scatterer whose SEM parameters are well known. It provides a convenient example for testing the general methods outlined in this report.

Our study produced two major results: The first is that the SEM parameters, including the natural frequencies, natural modes, coupling coefficients, and normalization factors can be calculated numerically from transient data generated with broad and narrow excitations. The second result is that by using signal averaging techniques, the SEM parameters can be calculated from simulated, noisy EMP test data.

CHAPTER II

FORMULATION

2.1 SEM FOR A THIN-WIRE SCATTERER

Consider a thin-wire scatterer with radius a and length L, assumed to lie along the z axis. The wire is struck by a plane electromagnetic wave. The direction of propagation $\bar{k}$ of the incident field makes an angle θ with the normal to the center of the scatterer as shown in Figure 1. The time origin is taken at the point where the incident wavefront peak is D_o meters from the midpoint of the scatterer. The incident field $\bar{E}$ is assumed to lie in the plane of the figure. The induced current on the scatterer for any θ and $0 \leq z \leq L$ is represented in [1] as

$$I(t,\theta,z) = \sum_{\alpha} R_{\alpha}(\theta,z)\, \exp(s_{\alpha}t)u(t-t_o) + g(t,\theta,z) \qquad (1)$$

where t_o is the turn-on time, the s_{α} are the natural frequencies or poles of the scatterer, the R_{α} are the corresponding residues at s_{α}, and $g(t,\theta,z)$ is the forced response. The summation over α represents the natural response of the scatterer. According to SEM the residues can be factored as

$$R_{\alpha}(\theta,z) = \eta_{\alpha}^{max}\eta_{\alpha}^{l}(\theta)i_{\alpha}(z)\tilde{f}(s_{\alpha}) \qquad (2)$$

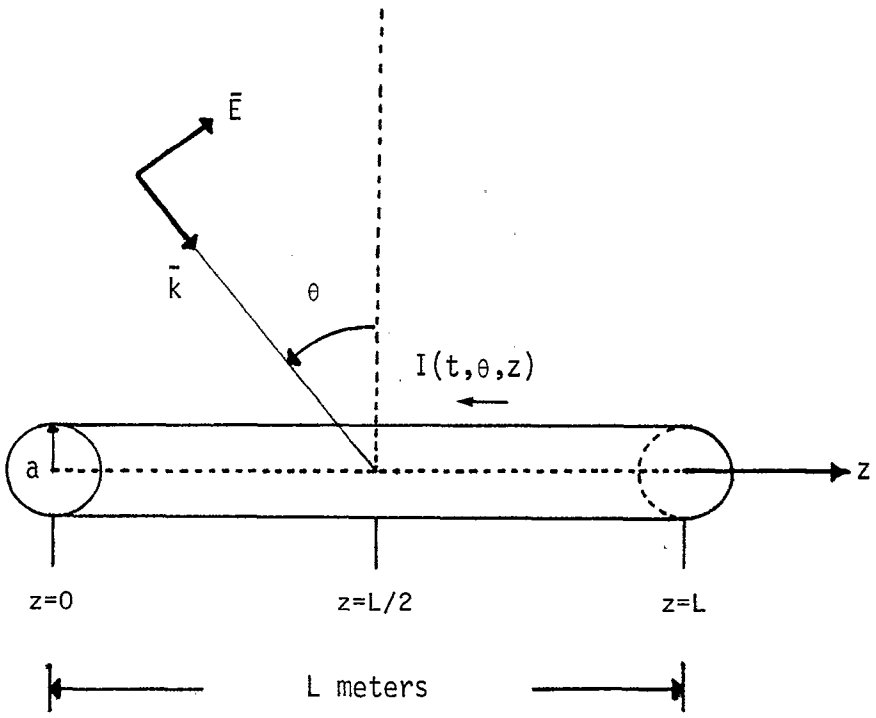

Figure 1. Geometry of the thin-wire scatterer and incident field

where

η_α^{max} - the normalization factor

η_α^{l} - normalized coupling coefficient

i_α - normalized natural mode

$\tilde{f}(s_\alpha)$ - Laplace transform of the exciting function

As a result, the natural response can be expressed in terms of SEM parameters as

$$\sum_\alpha R_\alpha(\theta,z)\exp(s_\alpha t)u(t-t_o) = \sum_\alpha \eta_\alpha^{max}\eta_\alpha^{l}(\theta)i_\alpha(z)\tilde{f}(s_\alpha)\exp(s_\alpha t)u(t-t_o) \tag{3}$$

Since the values of the induced current are always real, the poles s_α shown in Equation 1 occur in conjugate pairs or lie on the real axis of the complex s-plane. The poles have negative real parts and are generally assumed to be simple for a thin-wire scatterer. The pole values are uniquely determined by the wire radius and length.

The natural modes describe the spatial amplitude variation in the current. They are normalized so that at the maximum magnitude points they are real and equal to one. The modes are independent of the angle of incidence θ but are a function of the spatial coordinate z and the scatterer radius and length. In [6], the authors developed an approximate expression for the natural modes of a thin wire as

$$i_\alpha(z) = \sin(\alpha\pi z/L), \quad 0 \leq z \leq L, \quad \alpha = 1,2,3,..... \tag{4}$$

The coupling coefficients describe how the incident field couples to a scatterer. They depend on the angle of incidence θ and are independent of z. In [6], the coupling coefficients were approximated as

$$\tilde{f}(s_\alpha)\eta_\alpha^{max}\eta_\alpha^{l}(\theta) = \int_0^L \sin(\alpha\pi z/L)E_z^{inc}(z,s_\alpha)dz \qquad (5)$$

$E_z^{inc}(z,s_\alpha)$ is the Laplace transform of the incident tangential electric field along the scatterer and is given in [3] as

$$E_z^{inc}(z,s) = \tilde{f}(s)\cos(\theta)\ \exp(-sz\ \sin(\theta)/c) \qquad (6)$$

where c is the velocity of light. Hence, Equation 5 becomes

$$\eta_\alpha^{max}\eta_\alpha^{l}(\theta) = \int_0^L \sin(\alpha\pi z/L)\cos(\theta)\ \exp(-s_\alpha z\ \sin(\theta)/c)dz \qquad (7)$$

For convenience, the coupling coefficients are normalized so that at the maximum magnitude points they are real and equal to one. The normalization factor η_α^{max} determines the proper magnitude and phase in Equations 2, 5, and 7.

2.2 THE PROPERTIES OF THE EXCITING WAVEFORMS

In general, the induced currents on the scatterer can be viewed as the transient response to an incident EMP. Two incident waveforms with different properties were employed to generate the data used in this report. They are the Gaussian pulse and the double exponential pulse.

(1) The Gaussian Pulse

The Gaussian pulse can be used to obtain a wide bandwidth exciting function. It is given by

$$f_1(t) = \exp(-t^2/\sigma^2) \tag{8}$$

where σ is a constant. The Laplace transform of $f_1(t)$ is given by

$$\tilde{f}_1(s) = \sigma\sqrt{\pi}\, \exp(\sigma^2 s^2/4) \tag{9}$$

The Gaussian pulse has a broad frequency spectrum which resembles that of the delta function, except that the width of the latter is boundless, whereas that of the Gaussian pulse depends on the spread parameter σ. The bandwidth of the pulse increases with decreasing σ.

Since the Gaussian pulse cannot be represented by a low order sum of complex exponentials, care must be taken when analyzing the wire response with Prony's method [10]. One can wait until the exciting Gaussian waveform has effectively crossed the scatterer. Alternately, one can choose σ small enough that the pulse bandwidth is greater than the response bandwidth. In this case, to a good approximation the natural response of Equation 3 is the scaled impulse response and $g(t, \theta, z)$ is zero.

(2) The Double Exponential Pulse

The double exponential pulse is given by

$$f_2(t) = \gamma(e^{-\alpha t} - e^{-\beta t}) \qquad t \geq 0$$
$$= 0, \qquad \text{otherwise} \tag{10}$$

where β and α are the constants which determine the rising and decaying rates of the pulse. The field intensity γ is assumed to be unity. The Laplace transform of Equation 10 is

$$\tilde{f}_2(s) = \frac{1}{s + \alpha} - \frac{1}{s + \beta} \tag{11}$$

Since $f_2(t)$ is a sum of complex exponentials, Prony's method can be used for extracting response poles from the source driven region where the exciting waveform is still present. The poles due to the exciting pulse simply show up in the list of poles describing the response.

2.3 METHODS FOR CALCULATING THE SEM PARAMETERS

Two techniques were used to calculate the natural frequencies: Prony's method [7], [9], [13] and the iterative prefilter method [14]. Prony's method was used to analyze the "noiseless" response data generated by the thin-wire code. The method fits a sum of complex exponentials to a given current response. When the current actually is a sum of complex exponentials, the poles and residues computed are just those of the given response. Our experience has been that this method works very well with computer generated signals where the noise is small. With this kind of data it is easy to recognize the natural frequencies of the scatterer by simply increasing the number of exponentials fitted.

As the order increases, some pole values become approximately constant to several decimal places while others do not. Numerical errors in the computed response data cause some of the fitted pole values to continue changing. The poles that stabilize as the fitted order increases are the natural frequencies of the thin-wire.

In actual EMP test situations, errors occur in measuring the response of an object. Any practical scheme for calculating the SEM parameters must be able to tolerate some error in the data. There are a number of error sources [15]. One important error arises when an analog waveform is digitized. For simplicity, we will neglect other errors and model the digitizing error as a sequence of uncorrelated, zero mean, random variables added to samples of the current. Let the measured samples be given by

$$y(n) = I(n\Delta t,\theta,z) + e(n) \qquad n = 0,1,2,..... \qquad (12)$$

where $I(n\Delta t,\theta,z)$ is the wire current at sample $n\Delta t$ and $e(n)$ is the corresponding error. Prony's method can be used to estimate the poles of $I(n\Delta t,\theta,z)$ given $y(n)$. But it is necessary to use a number of extra poles to account for the noise. We have had better results using the iterative prefilter method [14]. Briefly, this technique initializes with Prony's method and then iteratively filters the data and improves the difference equation coefficient (and hence the pole) estimates. Our experience is that the prefilter technique gives better results than Prony's method when the data are noisy.

The calculation of the natural modes, coupling coefficients, and their normalization factors depends on the residues $R_\alpha(\theta,z)$ of Equation 2. These residues were calculated in the standard way [7] after the poles were calculated by either method above. It is worth mentioning that for noisy data case the residue estimates are unbiased if the poles are known exactly [16]. So the poles should be estimated as well as possible before the residues are calculated.

The data records $I(t,\theta,z)$ for all θ and z have the same poles. So there is a redundancy in the data that can be used to advantage. Also, since $R_\alpha(\theta,z)$ factors as a product of the natural mode and coupling coefficient, there is a redundancy in these parameters as well. Section 3.2 in Chapter III contains a discussion of how these two types of redundancy can be used to improve SEM parameter estimates. The averaging schemes described later depend on the assumption that error in the original data has zero mean. In a real test situation, systematic errors can often be noticed and corrected, so this assumption is reasonable.

CHAPTER III

NUMERICAL RESULTS

3.1 EVALUATION OF SEM PARAMETERS FROM NOISELESS DATA

3.1.1 The Transient Response

Since sufficient experimental data were not available we simulated data by running the time-domain thin-wire computer code WT-MBA/LLL1B [17]. The thin-wire scatterer was modeled using sixty equally-spaced segments. Two different exciting fields were used: the Gaussian pulse and the double exponential pulse. The geometry of the model is depicted in Figure 1. For both cases, plane wave excitation was assumed; D_o is the distance at $t = 0$ between the peak of the exciting pulse and the midpoint of the scatterer, and Δt is the width of each time step. These parameters appear in the thin-wire code. The numerical values for the parameters of the models are:

(1) The Gaussian Pulse Excitation

$$f_1(t) = \exp(-t^2/\sigma^2)$$

$$L = 1 \text{ meter}$$

$$\sigma = 2 \times 10^{-10} \text{ sec.}$$

$$a/L = 0.005$$

$$\Delta t = 5.556 \times 10^{-11} \text{ sec.}$$

$$D_o = 0.6 \text{ meter}$$

These parameter values were used in an example in [7].

(2) The Double Exponential Pulse Excitation

$$f_2(t) = (e^{-\alpha t} - e^{-\beta t})u(t)$$

$L = 10$ meters

$\alpha = 4 \times 10^6$

$\beta = 2.2 \times 10^8$

$a/L = 0.005$

$\Delta t = 5.556 \times 10^{-10}$ sec.

$D_o = 6$ meters

The transient response referred to was the induced current at the center of each of the sixty segments and was computed at 500 time-steps of width Δt. The SEM expression for the current is given by

$$I(t,\theta,z) = \sum_{\alpha} n_{\alpha}^{max} \eta_{\alpha}^{-1}(\theta) i_{\alpha}(z) \tilde{f}(s_{\alpha}) \exp(s_{\alpha} t) u(t-t_o) + g(t,\theta,z) \quad (13)$$

Some of these currents have been plotted in Figures 2 through 5, showing the θ dependence. In Figure 6 through 9 the effect of the variation of z is demonstrated. The time origin for these graphs was taken when the exciting pulse was D_o meters away from the wire center.

The damped oscillatory behavior of the response can be observed from all of the previously mentioned figures. The responses to the Gaussian pulse have more high frequency content than the responses to the double exponential pulse. This is expected from the properties of the exciting functions. The response to the Gaussian pulse in each case is roughly the impulse response scaled

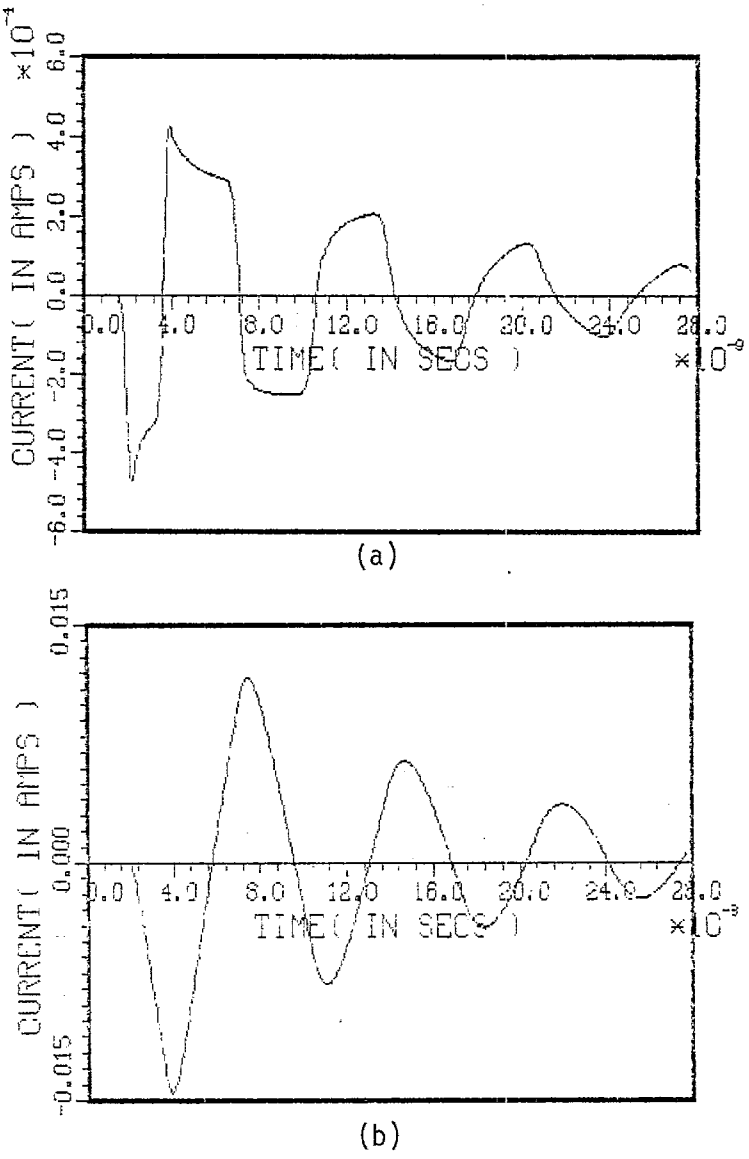

Figure 2. Response to (a) Gaussian pulse; (b) double exponential pulse at $\theta = 0°$, $z/L = 0.5$

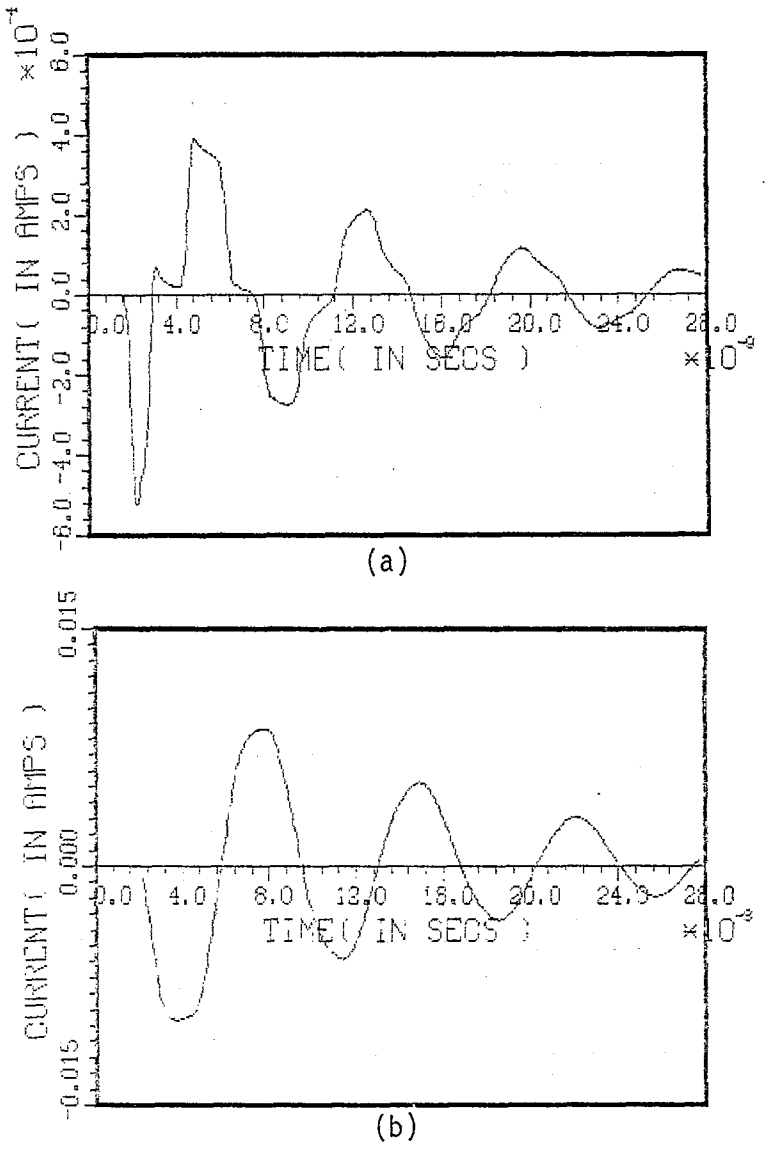

Figure 3. Response to (a) Gaussian pulse; (b) double exponential pulse at $\theta = 30°$, $z/L = 0.5$

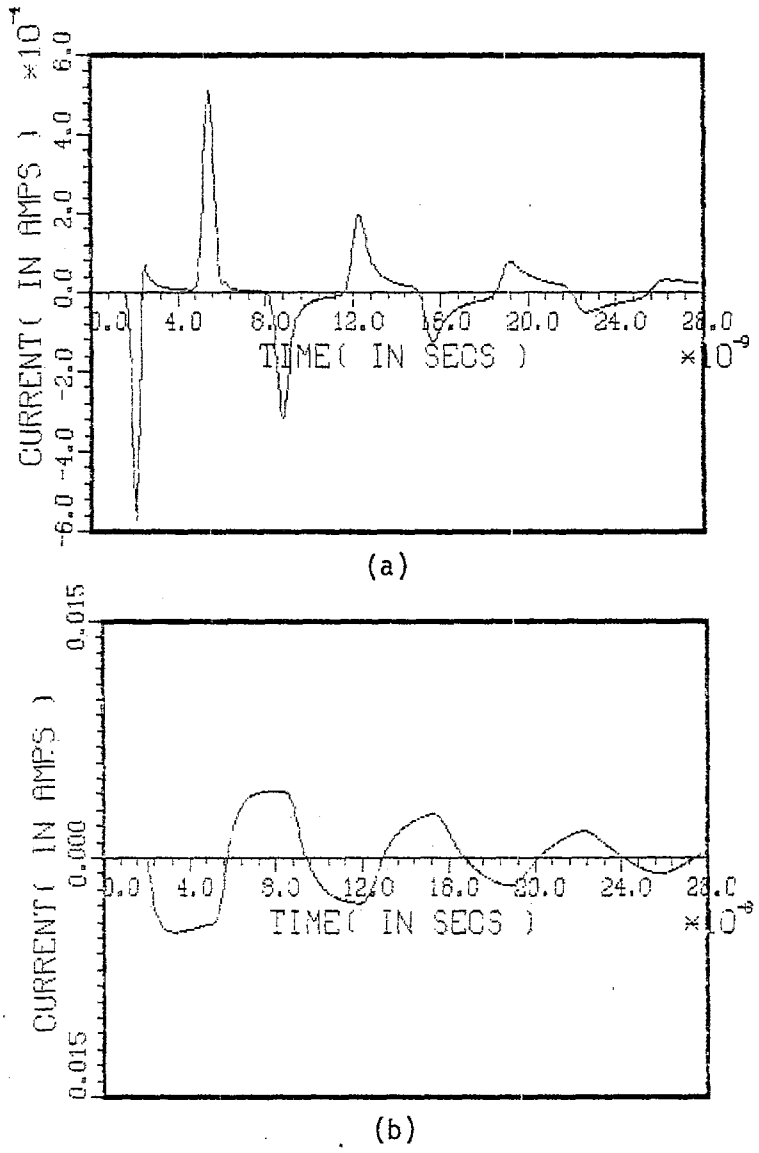

Figure 4. Response to (a) Gaussian pulse; (b) double exponential pulse at $\theta = 60°$, $z/L = 0.5$

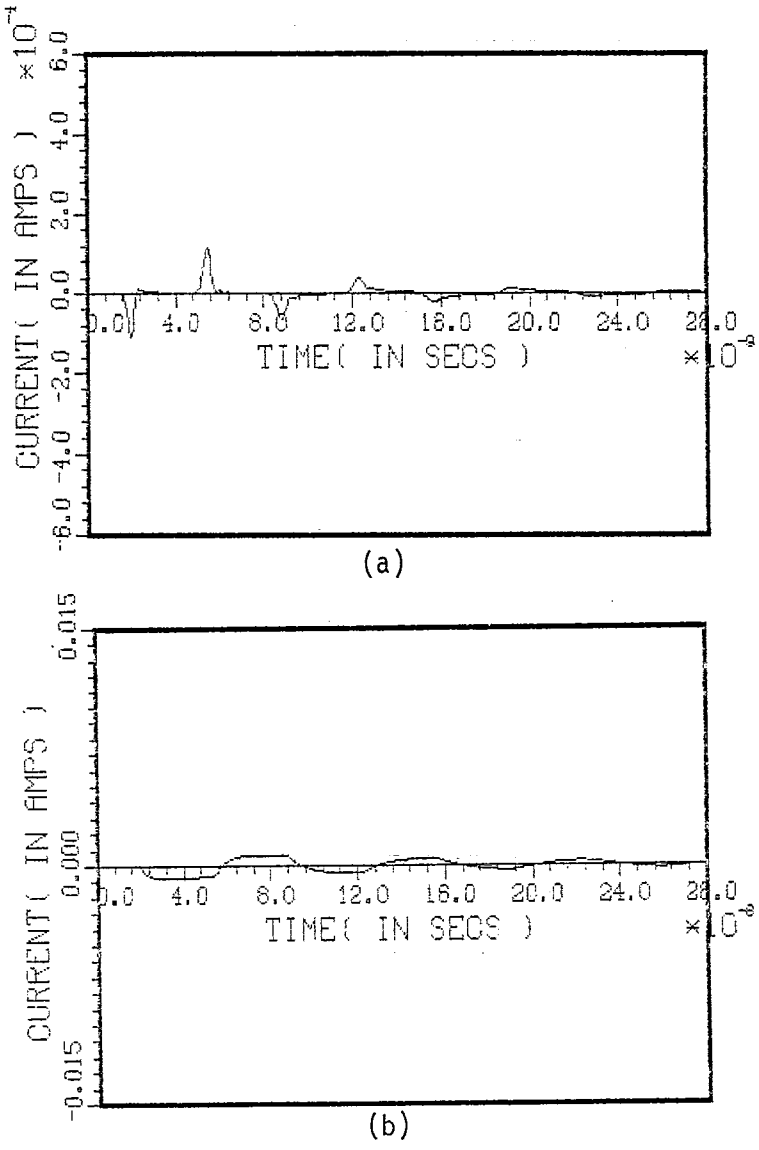

Figure 5. Response to (a) Gaussian pulse; (b) double exponential pulse at θ = 85°, z/L = 0.5

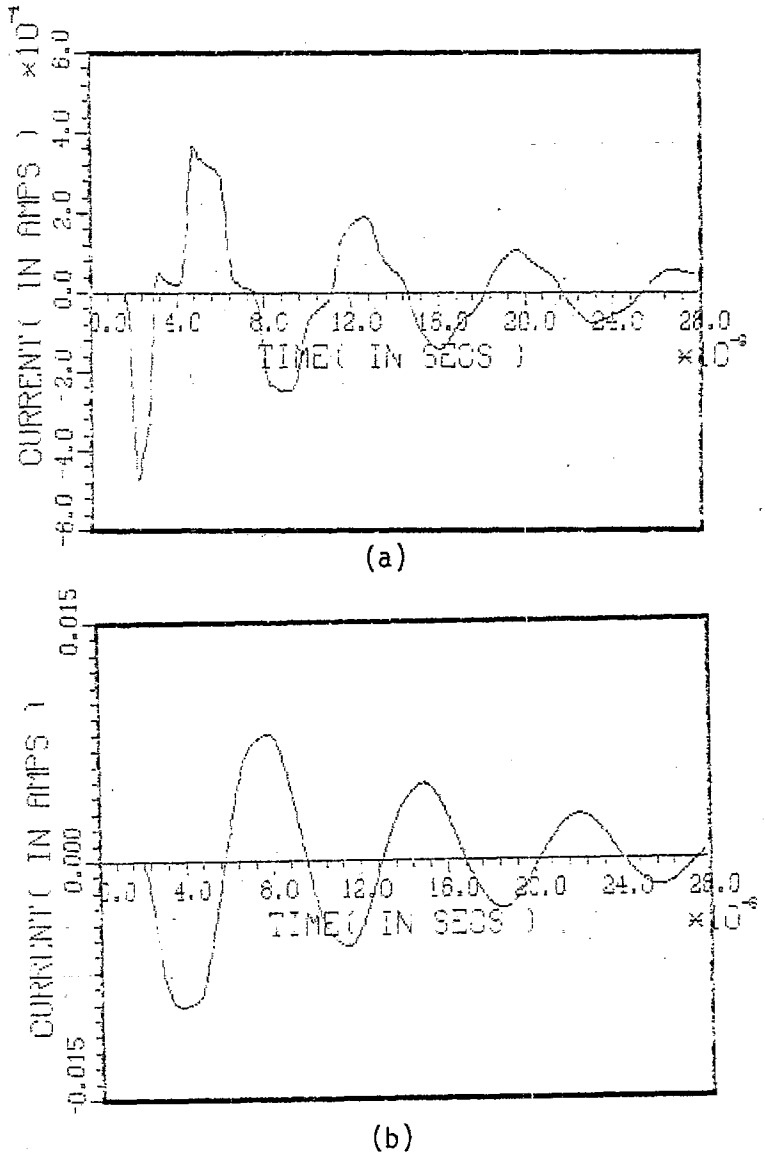

Figure 6. Response to (a) Gaussian pulse; (b) double exponential pulse at $\theta = 0°$, $z/L = 0.25$

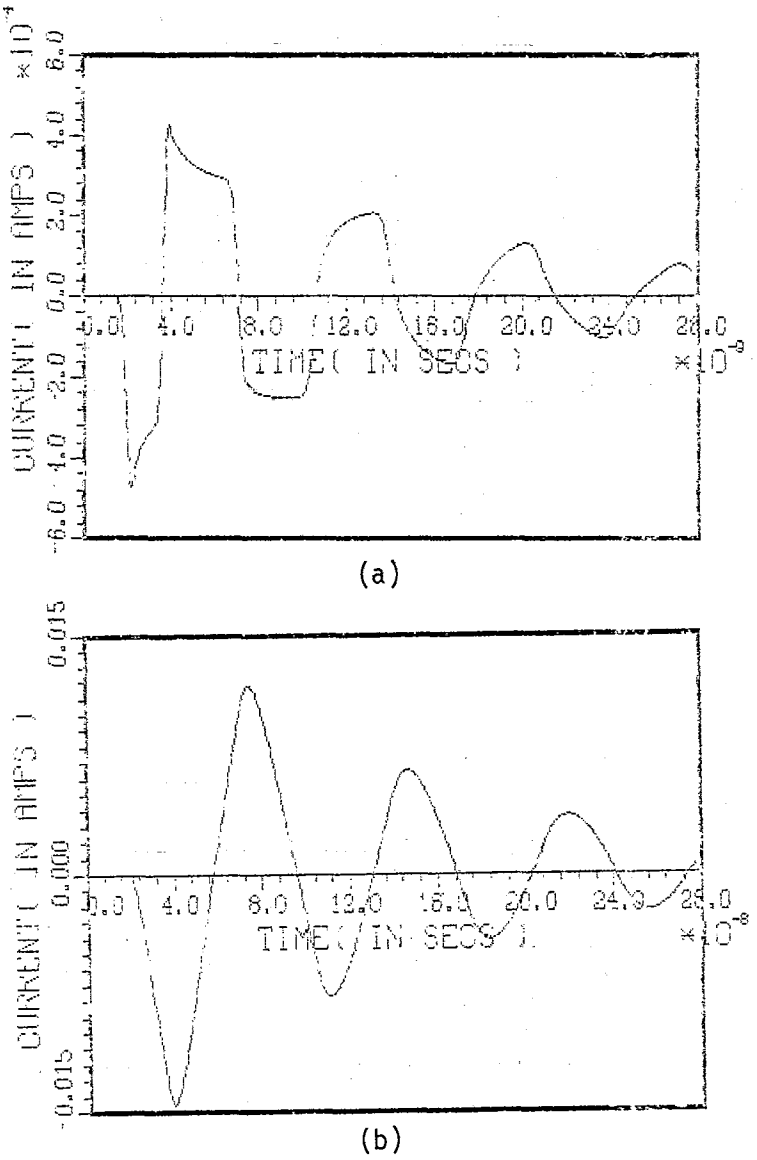

Figure 7. Response to (a) Gaussian pulse; (b) double exponential pulse at $\theta = 0°$, $z/L = 0.5$

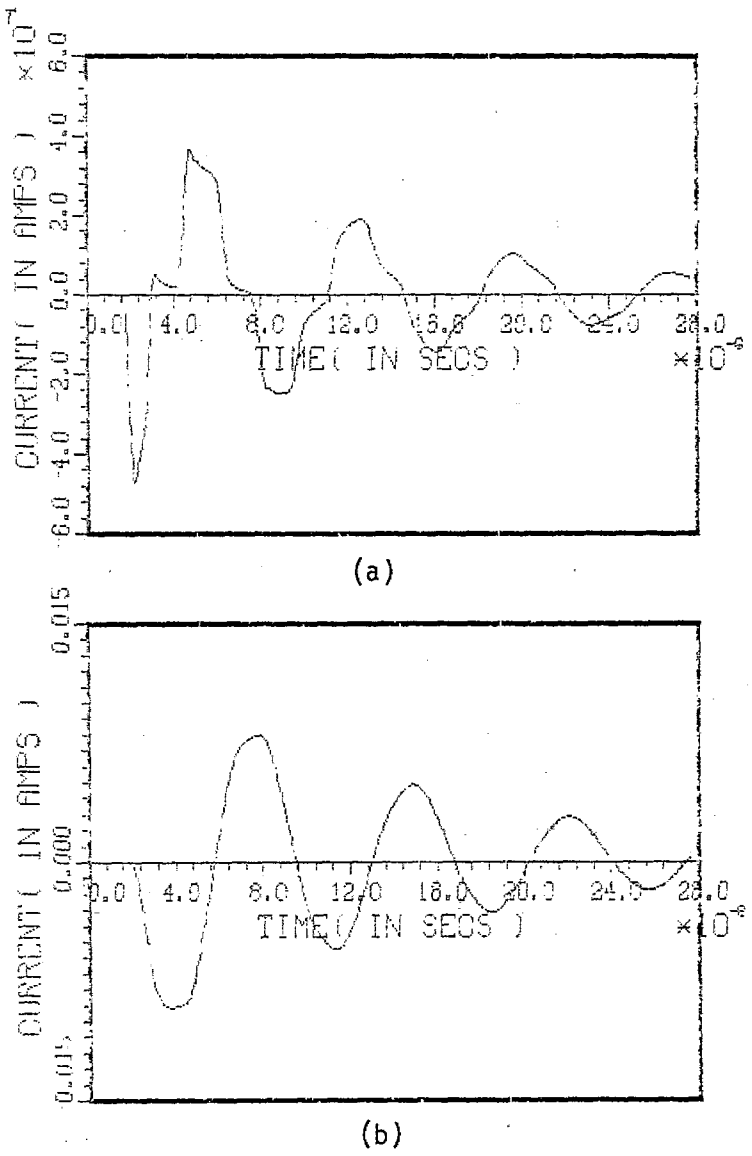

Figure 8. Response to (a) Gaussian pulse; (b) double exponential pulse at $\theta = 0°$, $z/L = 0.75$

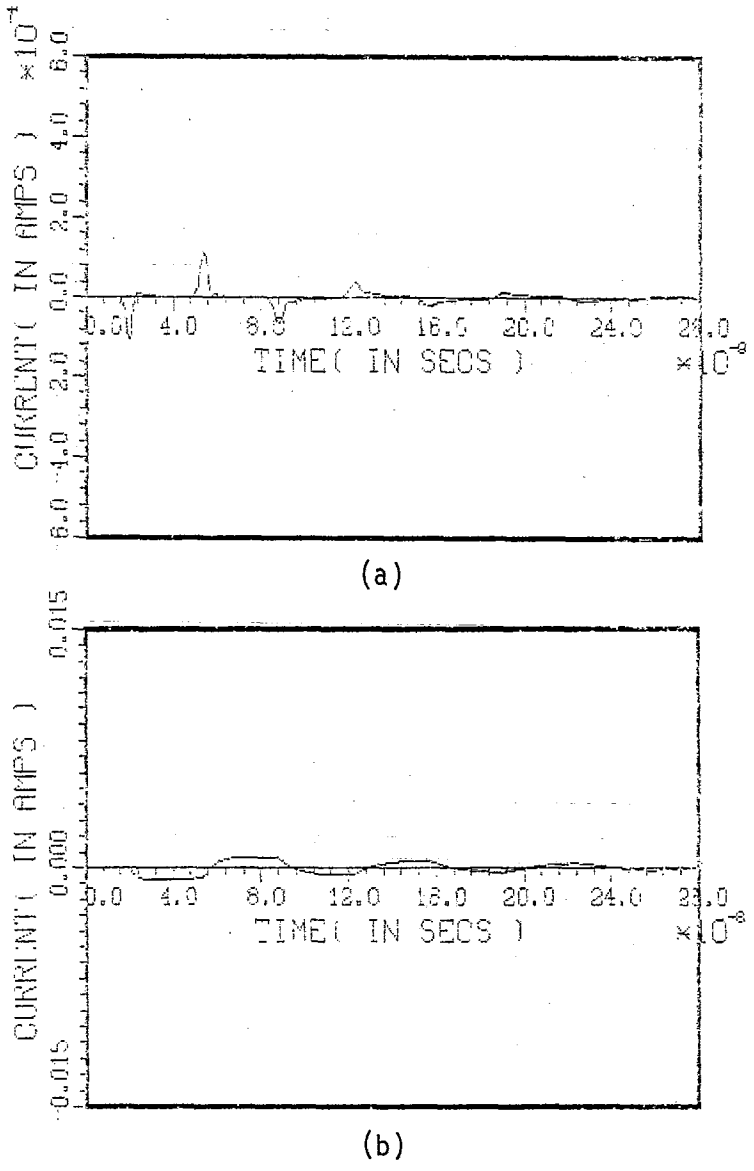

Figure 9. Response to (a) Gaussian pulse; (b) double exponential pulse at $\theta = 0°$, $z/L = 1.0$

by a constant. This is because the Gaussian pulse has a Fourier transform that is more or less flat up to the frequency of the seventh wire pole.

The responses at both ends of the scatterer are very insignificant. Theoretically, the responses are identically zero since the responses must satisfy the boundary conditions for the E-field integral equation of the thin-wire problem [6].

$$I(t,\theta,0) = I(t,\theta,L) = 0 \qquad (14)$$

With broadside incidence ($\theta = 0°$), the electric field is parallel to the wire and only symmetric modes are excited. In this case, the response starts exactly at the same time ($=D_o/c$ sec.) for all sixty segments.

Also, as the incident field angle approaches 90 degrees, the response tends to be weakened. This is because the exciting wave travels in the direction of z, parallel to the scatterer. Thus, no resonance will be excited on the scatterer as expected.

3.1.2 The Natural Frequencies and the Corresponding Residues

When the thin-wire code was run on the CDC 7600 computer, thirteen decimal precision was requested. Hence, the output data records can be considered practically noise free. The Prony program was used for extracting poles and calculating the residues successively from the output data.

Table 1 shows the natural frequencies obtained by running the Prony program on the response data with the Gaussian pulse excitation.

Table 1

First Ten Layer One Poles

N	SGB[1]	Tesche[2]	Prony's Method
1	-0.0828 + j0.9251	-0.082 + j0.926	-0.0819 + j0.919
2	-0.1212 + j1.9117	-0.120 + j1.897	-0.1210 + j1.896
3	-0.1491 + j2.8835	-0.147 + j2.874	-0.1490 + j2.879
4	-0.1713 + j3.8741	-0.169 + j3.854	-0.1717 + j3.866
5	-0.1909 + j4.8536	-0.188 + j4.835	-0.1916 + j4.852
6	-0.2080 + j5.8453	-0.205 + j5.817	-0.2093 + j5.839
7	-0.2240 + j6.8286	-0.220 + j6.800	-0.2256 + j6.821
8	-0.2383 + j7.8212	-0.234 + j7.783	-0.2386 + j7.794
9	-0.2522 + j8.8068	-0.247 + j8.767	-0.2575 + j8.775
10	-0.2648 + j9.8001	-0.260 + j9.752	-0.2951 + j9.735

[1][18] by Singaraju, Giri, and Baum

[2][3] by Tesche

[3]with the Gaussian pulse at $\theta = 60°$ and $z/L = 0.5$

The results reported by [3] and [18] were also tabulated. When the first ten poles were compared, our results agreed very well with the others. These pole values are essentially independent of the starting time for the analysis and also of the segment number and

angle of incidence provided the corresponding modes are excited. The same kind of results are obtained when the double exponential pulse is used except of course that two extra poles are present. It is interesting that Tesche's analysis [3] found two layers of poles but our approach found poles from only the first layer.

The poles and residues found can be used to approximate the original waveform. Figure 10 shows the reconstructed responses to both excitations at 0 degrees incident angle. Nine wire pole pairs were used. The corresponding transforms are shown separately in Figures 11 and 12. In the case of this response to the double exponential pulse, only two wire pole pairs are actually needed to provide an accurate reconstruction of the original response. Of course, the number of pole pairs needed in the reconstruction is a function of the frequency content of the original response. This frequency content depends on the values of the natural modes, coupling coefficients, and incident field spectrum.

3.1.3 The Natural Modes

For a fixed $\theta = \theta'$, Equation 2 can be rewritten as

$$R_\alpha(\theta',z) = \eta_\alpha^{max}\eta_\alpha^{l}(\theta')i_\alpha(z)\tilde{f}(s_\alpha), \qquad 0 \le z \le L \qquad (15)$$

The coupling coefficient term in Equation 15 is merely a constant now. As z is varied from 0 to L, $R_\alpha(\theta',z)$ is simply proportional to the natural mode current $i_\alpha(z)$. This proportionality may be removed by normalizing the maximum value of each mode to unity.

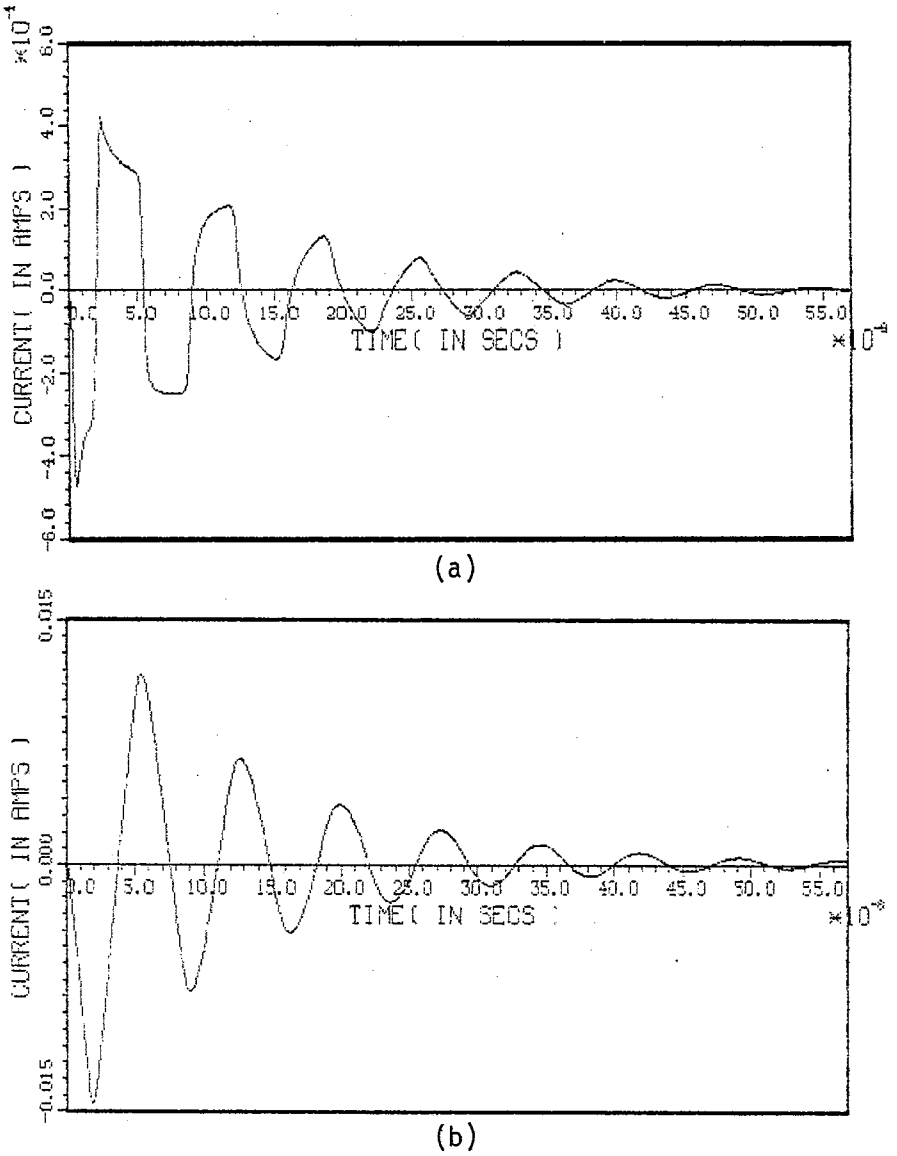

Figure 10. Reconstructed response to (a) Gaussian pulse; (b) double exponential pulse, at $\theta = 0°$, $z/L = 0.5$

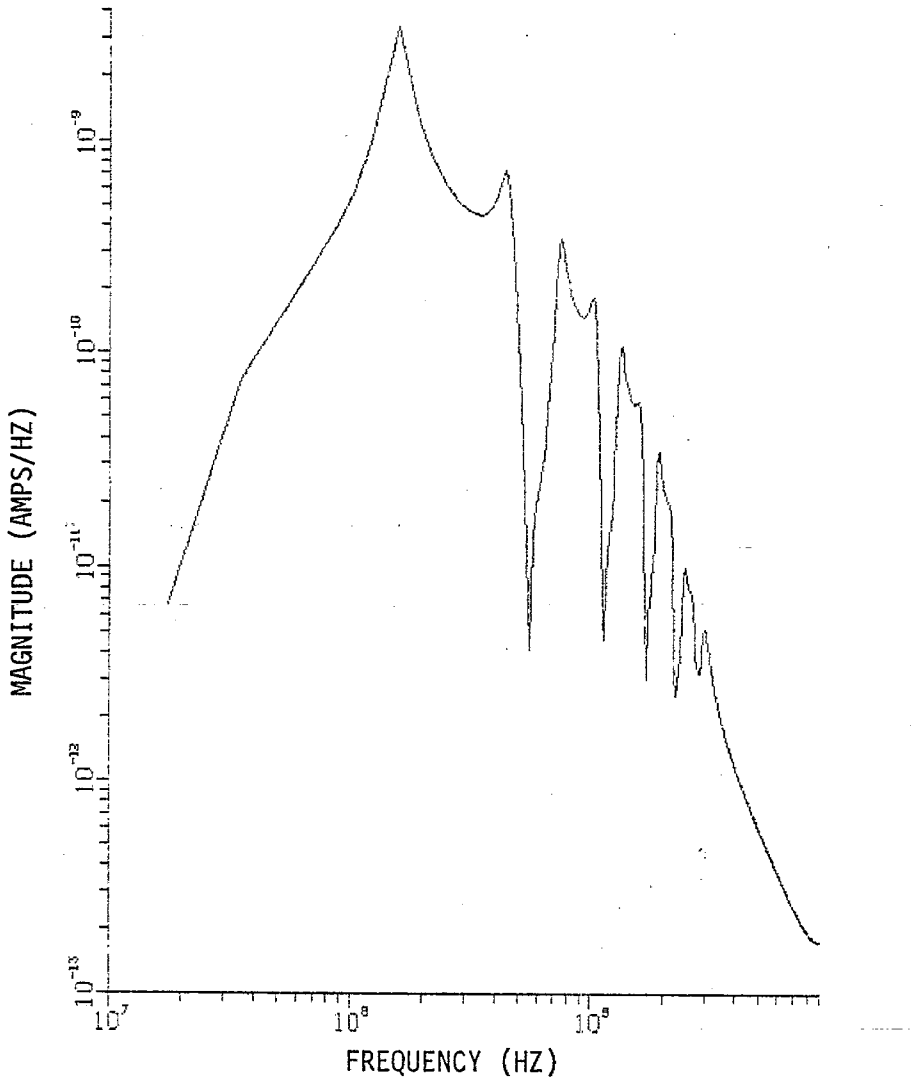

Figure 11. Fourier transform magnitude of reconstructed response to Gaussian pulse at $\theta = 0°$, $z/L = 0.5$

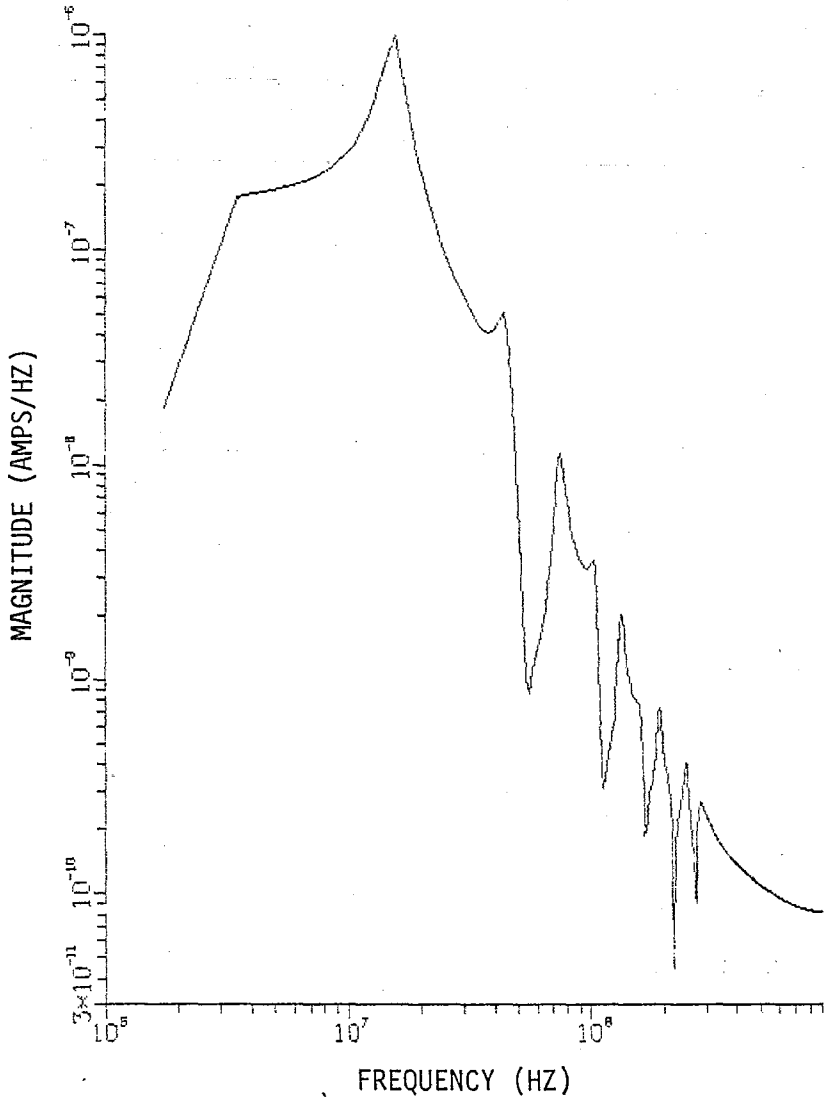

Figure 12. Fourier transform magnitude of reconstructed response to double exponential pulse at $\theta = 0°$ and $z/L = 0.5$

The normalized natural modes for the first three resonances are plotted in Figures 13 through 18. It is observed that the natural modes are either symmetric or anti-symmetric about the center of the scatterer. When the field is normally incident on the scatterer, only even modes are excited as expected.

These results are virtually identical with those obtained by Tesche [3] and by Pearson and Robertson [13].

3.1.4 The Coupling Coefficients

As can be seen from Equation 2, the coupling coefficients contain the θ variation of the residues. For a fixed z we calculated the residues for several different θ. The value of z can be chosen from the normalized natural mode plot so that the peak of each mode corresponds to the chosen position of z on the scatterer. The normalized variation in these residues gives the $n_\alpha^1(\theta)$.

The normalized coupling coefficients for the first three resonances are presented in Figures 19 and 21 for both excitations with both real and imaginary parts shown. In Figure 20, the imaginary part (Gaussian excitation) is shown alone.

It should be noted that we normalized the coupling coefficients so that the maximum magnitude points are real and equal to one. This is convenient when handling experimental data since the underlying integral equation is unknown. Tesche normalized the coupling coefficients differently since he knew the integral equation. Thus different versions of the plots were obtained.

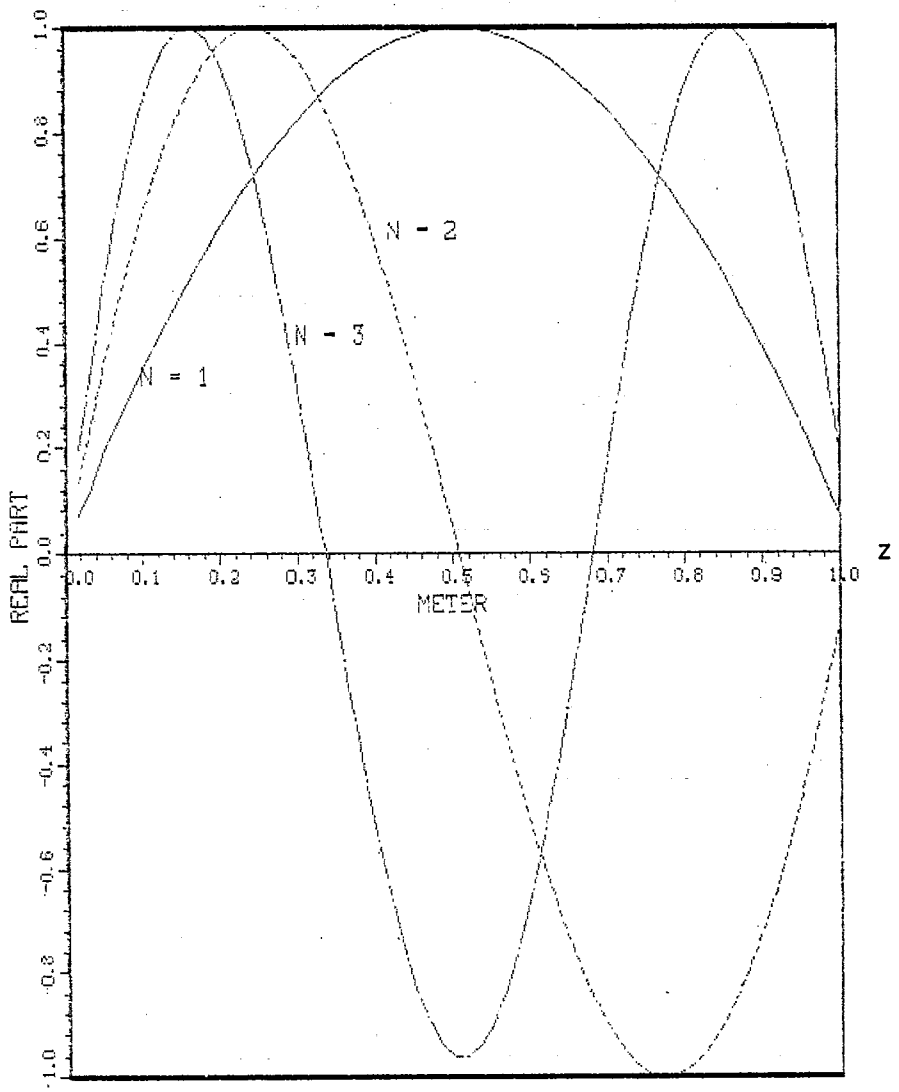

Figure 13. Real parts of first three normalized natural modes for thin wire, a/L = 0.005 (Gaussian pulse excitation at $\theta = 60°$)

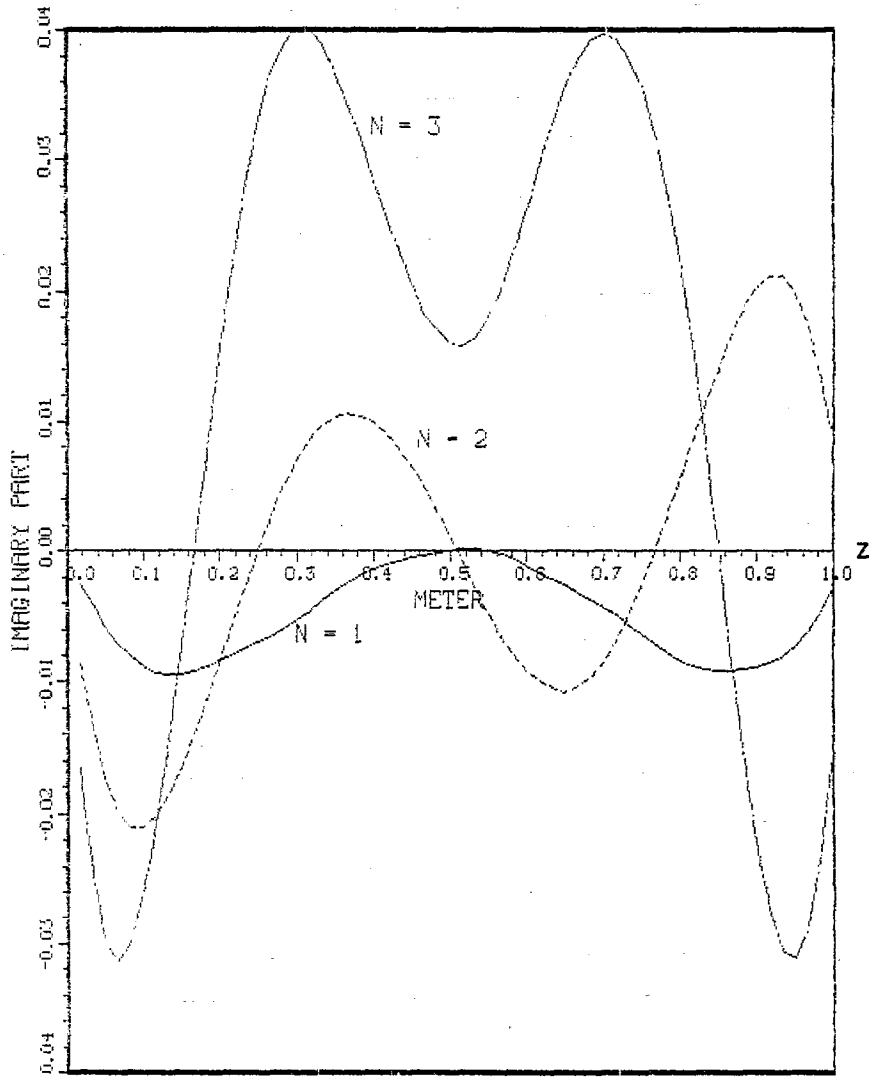

Figure 14. Imaginary parts of first three normalized natural modes for thin wire, a/L = 0.005 (Gaussian pulse excitation at $\theta = 60°$)

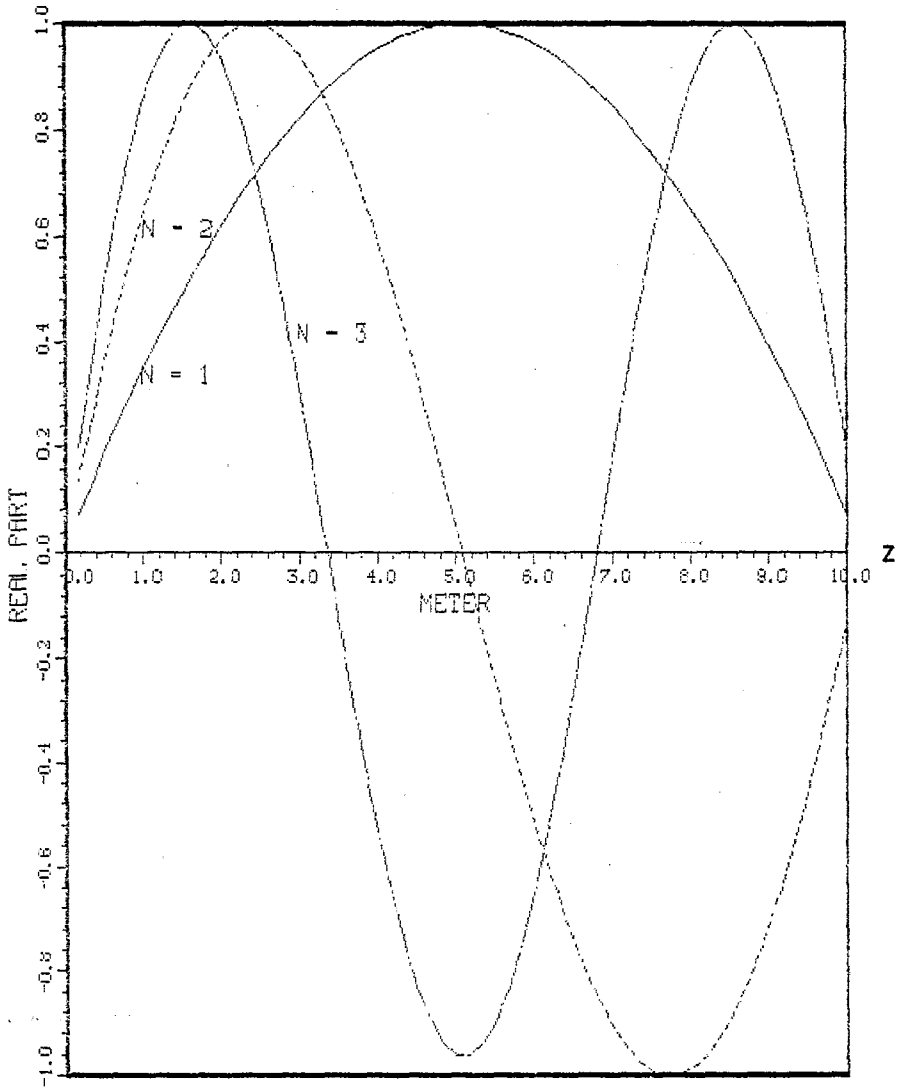

Figure 15. Real parts of first three normalized natural modes for thin wire, a/L = 0.005 (double exponential pulse excitation at $\theta = 60°$)

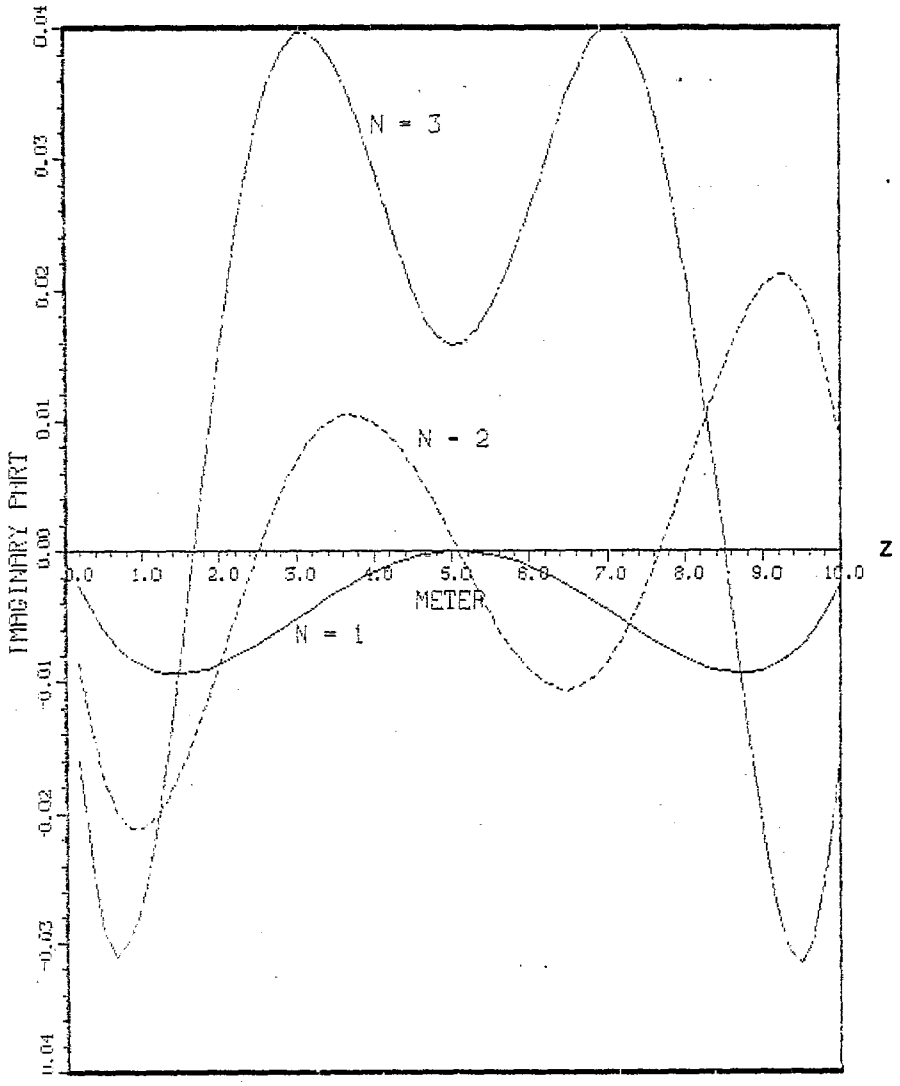

Figure 16. Imaginary parts of first three normalized natural modes for thin wire, a/L = 0.005 (double exponential excitation at $\theta = 60°$)

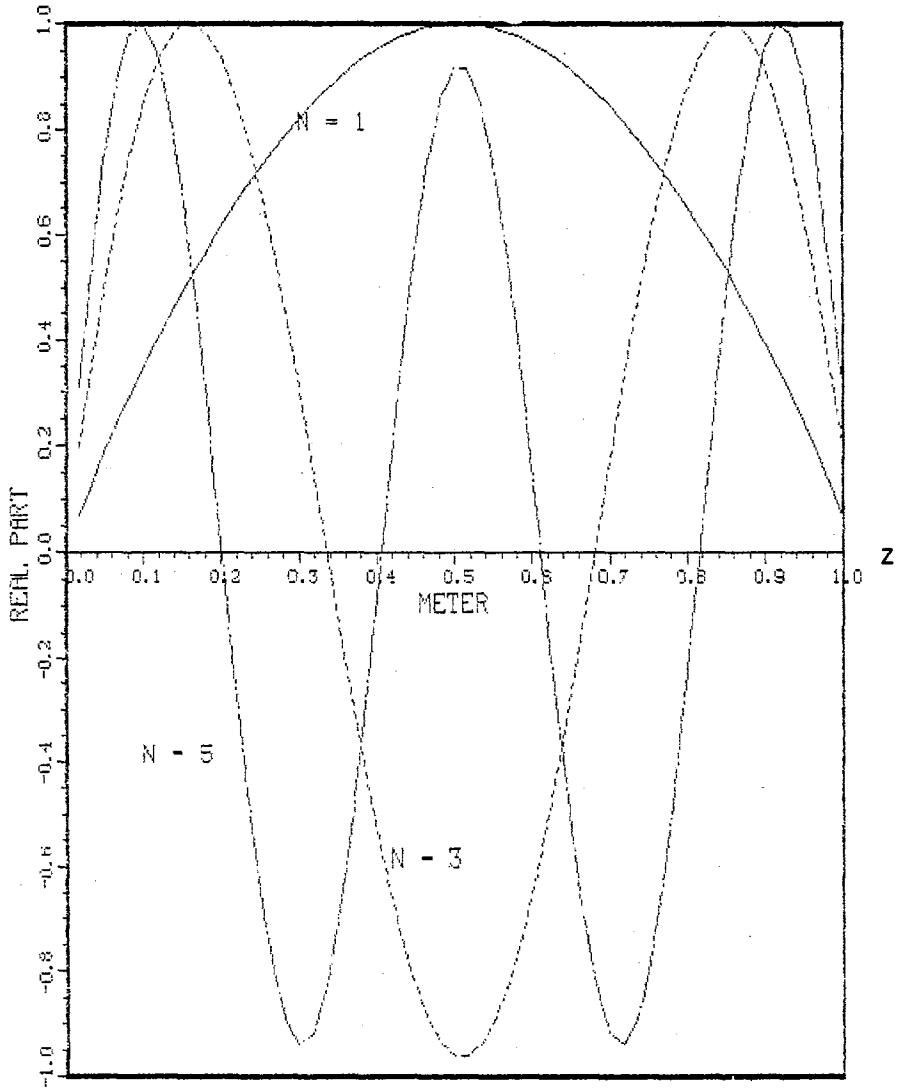

Figure 17. Real parts of first three normalized natural modes of thin wire, a/L = 0.005 (Gaussian pulse excitation at $\theta = 0°$)

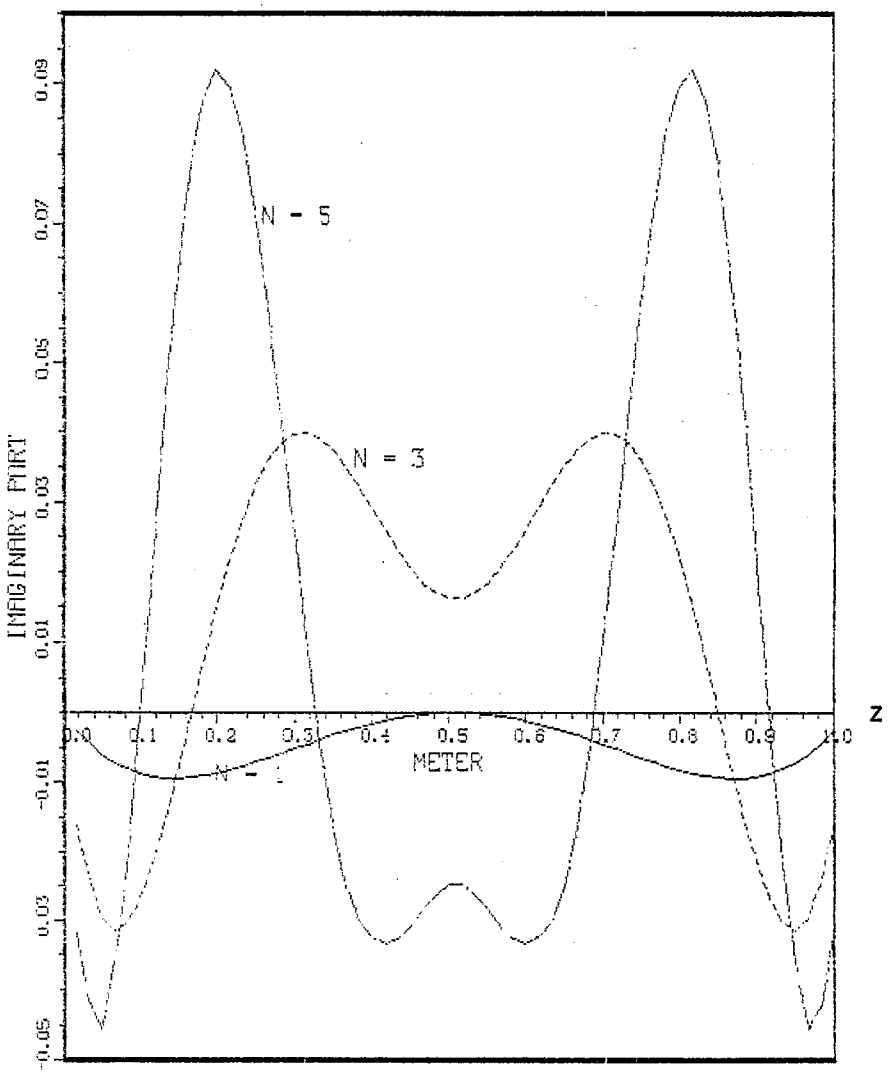

Figure 18. Imaginary parts of first three normalized natural modes of thin wire, a/L = 0.005 (Gaussian pulse excitation at $\theta = 0°$)

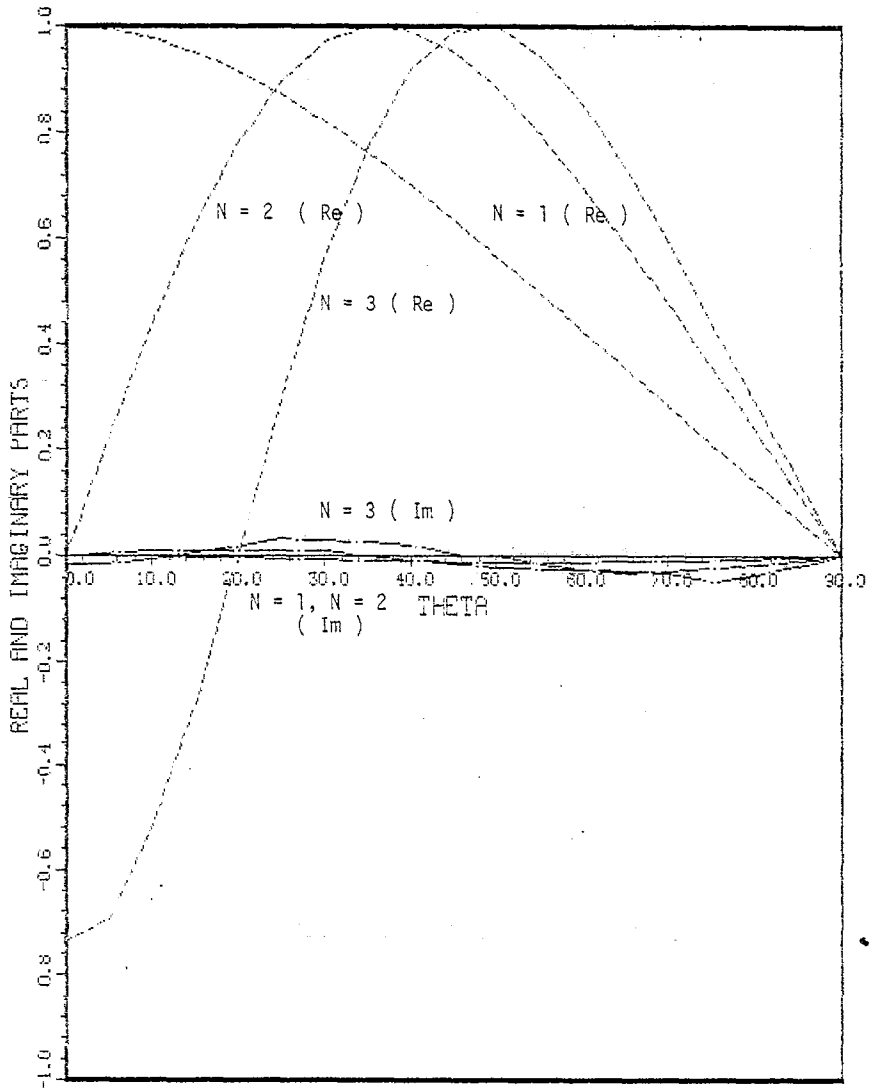

Figure 19. Normalized coupling coefficients calculated using Gaussian excitation, both real and imaginary parts of first three modes, are shown

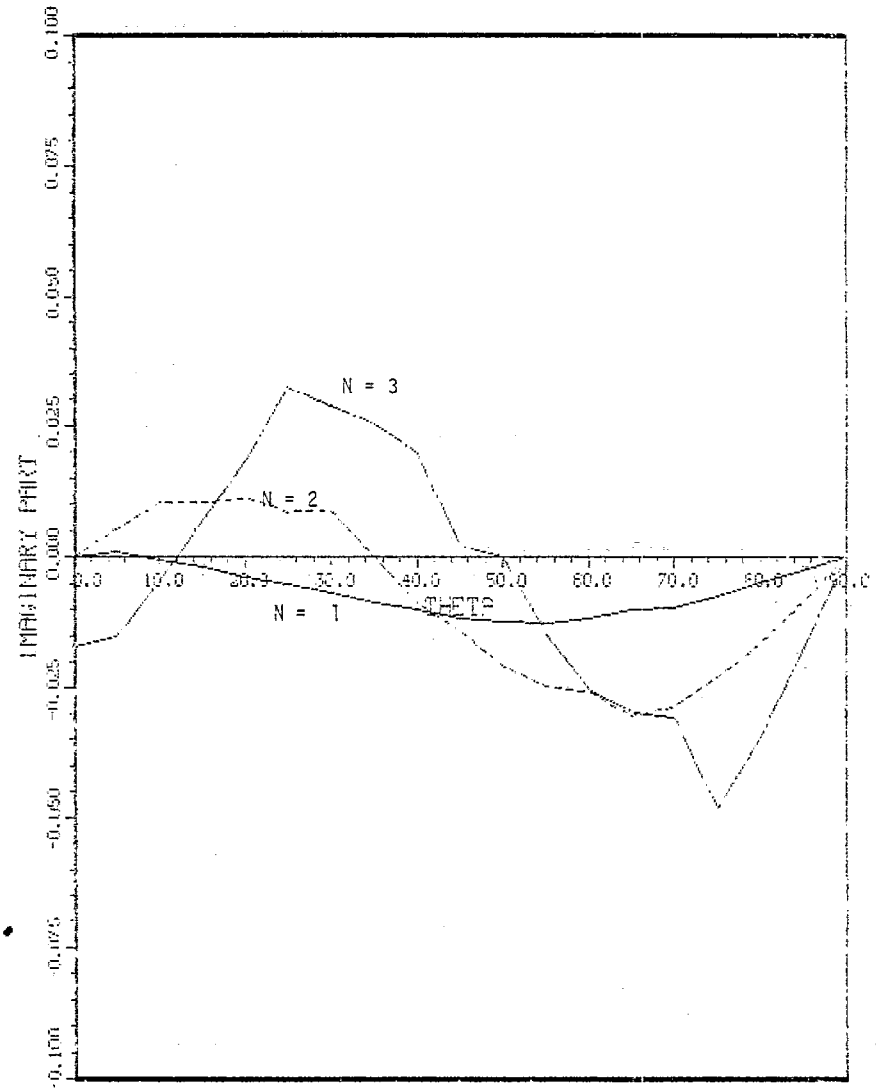

Figure 20. Imaginary parts of first three modes of normalized coupling coefficients (Gaussian excitation)

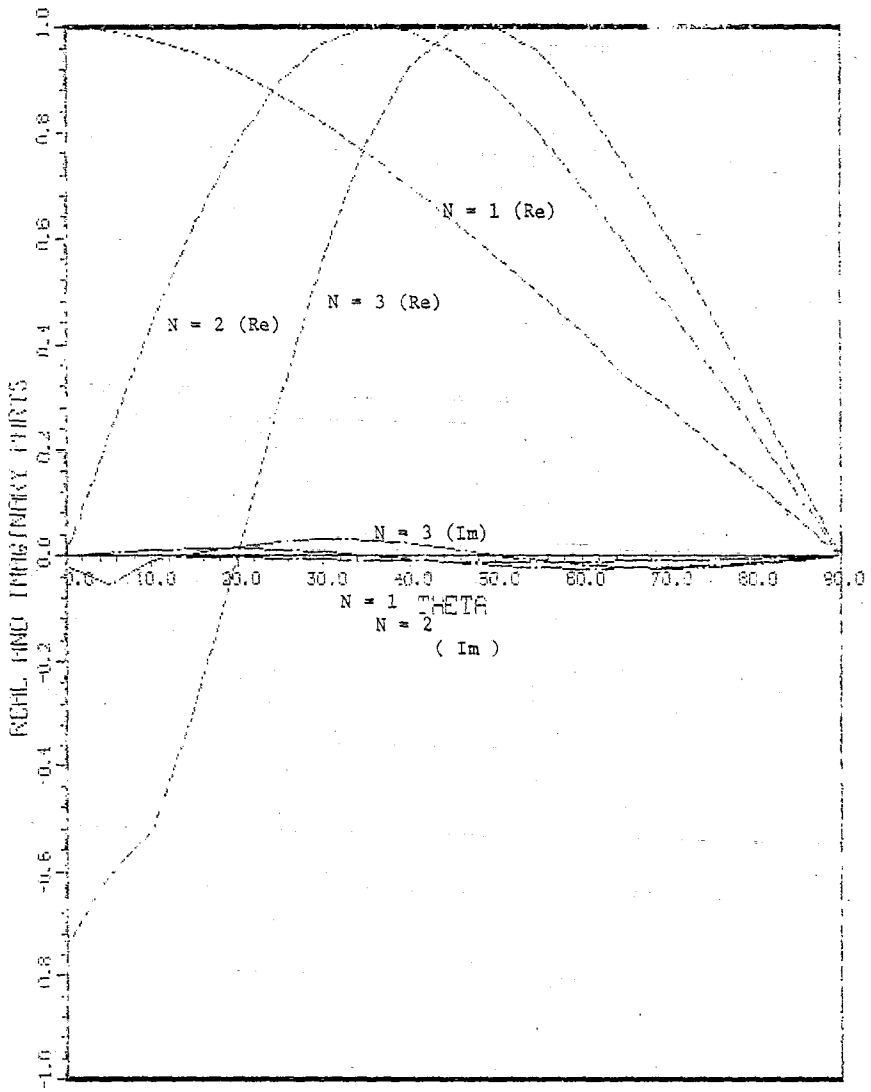

Figure 21. Normalized coupling coefficients calculated using double exponential excitation, both real and imaginary parts of first three modes, are shown

As can be observed from the graphs, the imaginary parts of the coupling coefficients are relatively small and this implies that the coupling coefficients are almost real functions of the incident angle θ. The graphs would be smoother if more values of $\eta_\alpha^1(\theta)$ had been computed. Only nineteen values of θ were used for each graph in Figures 19, 20 and 21.

3.1.5 The Normalization Factors

Now all the SEM parameters, except the normalization factors, in Equation 2 are known. This final parameter may be determined directly from Equation 2 by means of simple complex arithmetic, i.e.,

$$\eta_\alpha^{max} = \frac{R_\alpha(\theta,z)e^{s_\alpha t_1}}{\eta_\alpha^1(\theta)i_\alpha(z)\tilde{f}(s_\alpha)} \quad , \qquad \text{for } 0 \le z \le L \qquad (16)$$

The normalization constant contains an arbitrary factor t_1 that depends on the choice of the time origin. In all the preceding graphs, the time origin was chosen so that at $t = 0$ the incident field peak was D_0 meters from the wire center. D_0 is arbitrary and is chosen for convenience in running the thin-wire code. However, it is better to eliminate D_0 from η_α^{max} and have it depend on the shape of the scatterer. For this reason, we multiplied the residues $R_\alpha(\theta,z)$ by a time shift factor to move the time origin to the time when the incident pulse peak crosses the wire center. The required factor is $e^{s_\alpha t_1}$, where

$$t_1 = D_o/c - t_s \tag{17}$$

and where t_s is the time at which we started to analyze the transient response. In our calculations, t_s was chosen at the 210^{th} time step to ensure all the observed responses had started. So $t_s = 210\ (\Delta t)$.

The normalization factors for the first three modes of both excitations are:

1. The Gaussian Excitation

$$\eta_1^{max} = -0.7072779\times10^6 - j0.1938136\times10^6 \quad (\theta=0°, z/L=0.5)$$

$$\eta_2^{max} = 0.1431957\times10^6 - j0.4662369\times10^6 \quad (\theta=60°, z/L=0.25)$$

$$\eta_3^{max} = 0.3933103\times10^6 + j0.1275519\times10^6 \quad (\theta=0°, z/L=0.17)$$

2. The Double Exponential Excitation

$$\eta_1^{max} = -0.7075146\times10^6 - j0.1935304\times10^6 \quad (\theta=0°, z/L=0.5)$$

$$\eta_2^{max} = 0.1421189\times10^6 - j0.4659009\times10^6 \quad (\theta=60°, z/L=0.25)$$

$$\eta_3^{max} = 0.3911535\times10^6 + j0.1245812\times10^6 \quad (\theta=0°, z/L=0.17)$$

Since the normalization factor is merely a scaling complex constant for each pole, it is independent of either θ or z. The results obtained are very close for both excitations.

Tesche [3] normalized the coupling coefficients differently, therefore his normalization factors are different from what we computed.

3.2 THE EFFECTS OF NOISE ON SEM PARAMETER DETERMINATION

3.2.1 The Effect of Noise on the Transient Responses

The simulated EMP data were obtained by adding sequences from the CDC 6600 random number generator to the data computed by the thin-wire code. The noise sequence was assumed to be uniformly distributed with (statistical) mean zero and standard deviation scaled to one and one half percent of the peak value of each data record. This is about the level of digitizing noise encountered in actual testing.

Sample noise corrupted responses ($\theta=0°, z/L=0.5$) are presented in Figure 22 for both excitations. The corresponding Fourier transform magnitudes are shown in Figures 23 and 24.

Both signals contain the 1.5 percent standard deviation noise. More signal peaks are visible in the Gaussian response spectrum. This is because the wide bandwidth Gaussian pulse puts more energy into the higher frequency modes than does the double exponential pulse.

3.2.2 The Effect of Noise on the Natural Frequencies and the Residues

The direct computation of the poles from noisy transient data can lead to inaccurate results. Besides, only a limited number of system poles can be extracted, since the rest have been severely corrupted by noise. In principle, each response record

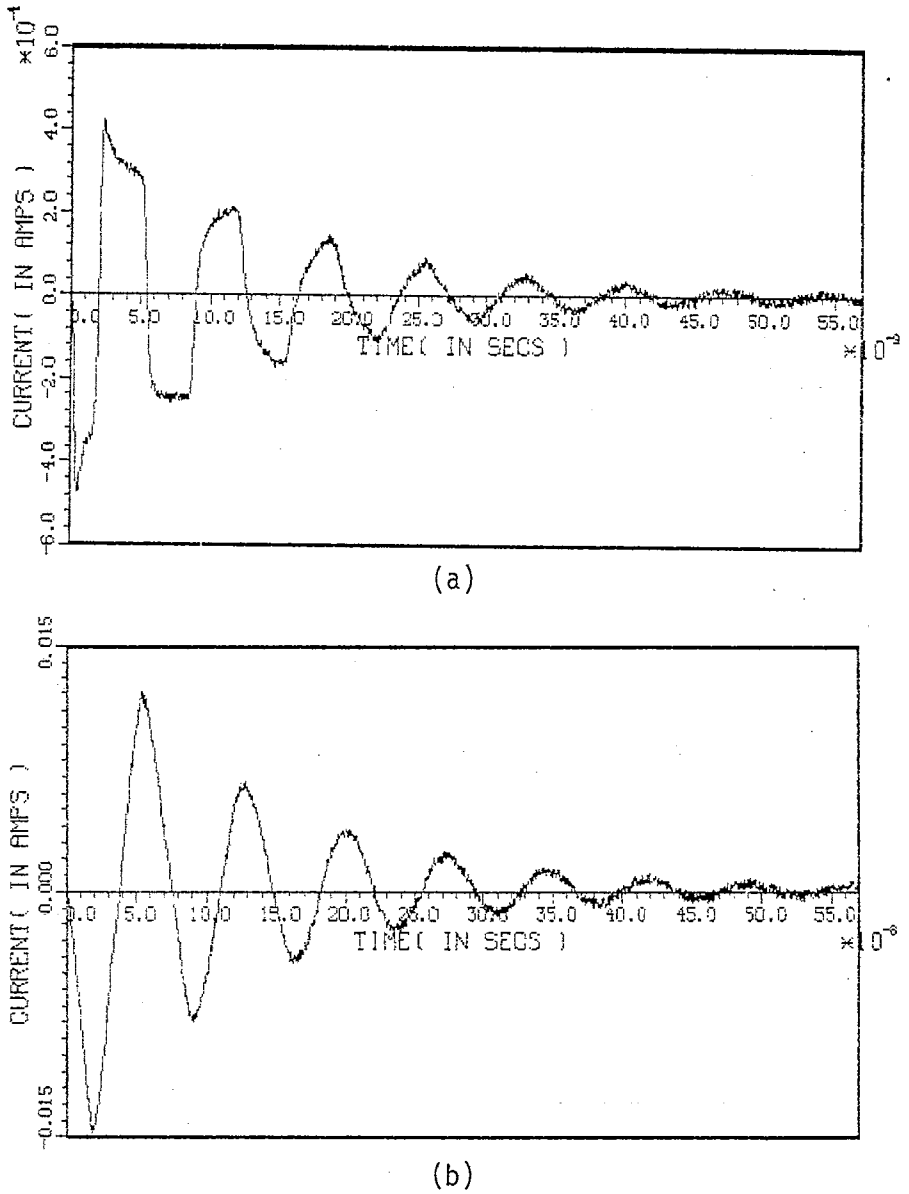

Figure 22. Noise corrupted response to (a) Gaussian, (b) double exponential pulse, at $\theta = 0°$, $z/L = 0.5$

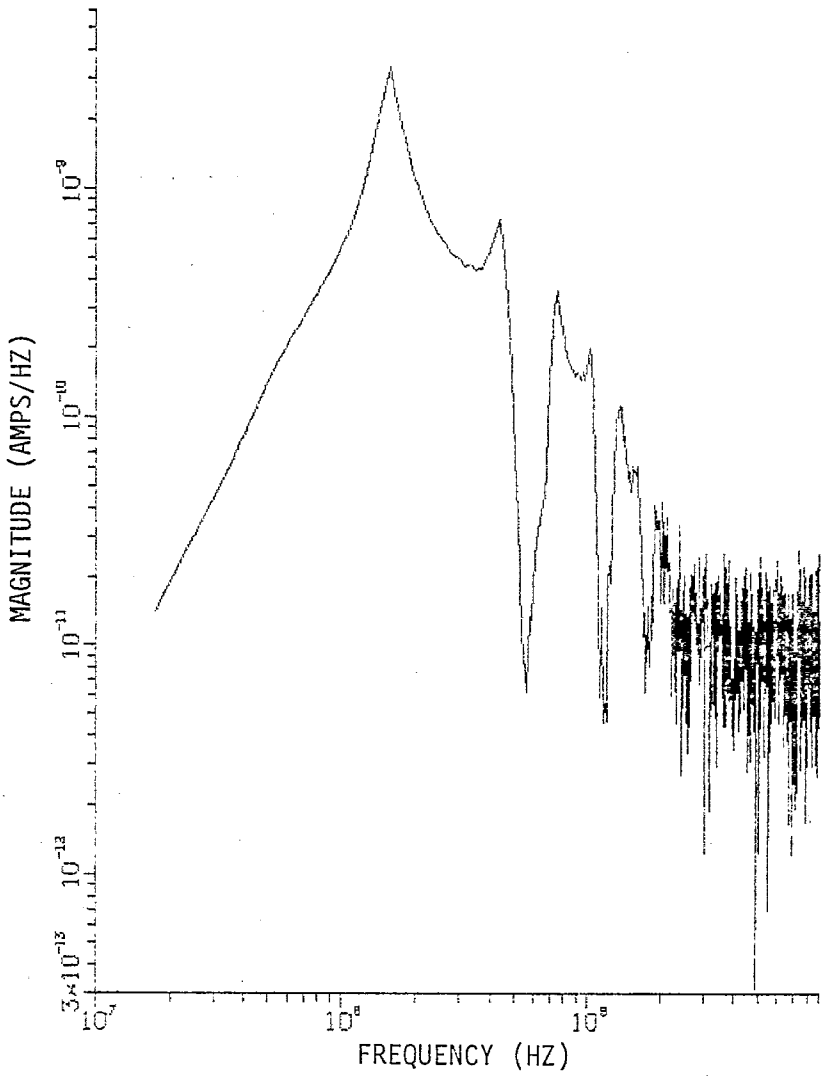

Figure 23. Fourier transform magnitude of noise corrupted response to Gaussian pulse at $\theta = 0°$, $z/L = 0.5$

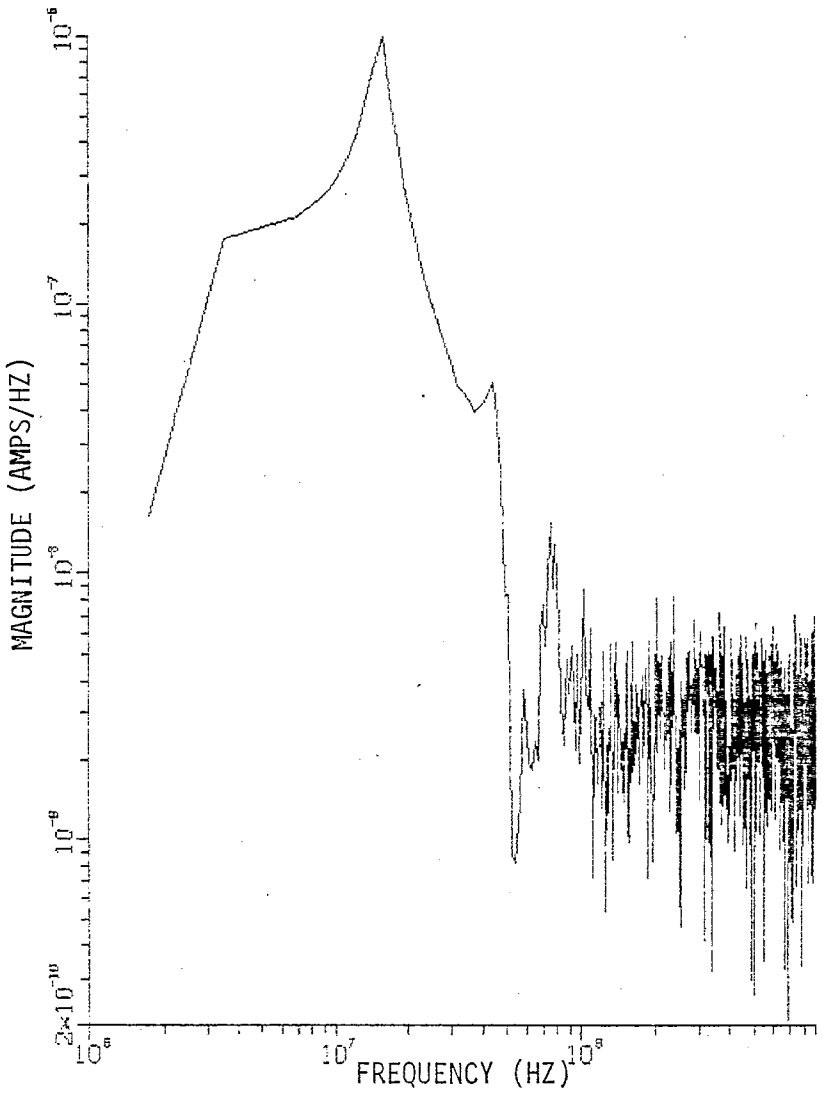

Figure 24. Fourier transform magnitude of noise corrupted response to double exponential pulse at $\theta = 0°$, $z/L = 0.5$

contains the same poles. It is possible to use extra data to enhance a particular natural frequency.

The iterative prefilter method rather than Prony's method was used for all the pole estimates in this section. Suppose data $y(t,\theta,z)$ is available at several θ and z values. Poles can be computed from each of the records resulting in estimates $\hat{s}_\alpha(\theta,z)$. The arguments θ and z are included to show that the pole estimates depend on location and angle of incidence. Of course the actual wire poles are independent of θ and z. Usually some of the pole estimates cluster, that is, the values lie close together in the s-plane. An estimate of s_α can be computed as the average over a cluster.

$$\hat{s}_\alpha = \frac{1}{N} \sum_{\theta} \sum_{z} \hat{s}_\alpha(\theta,z) \tag{18}$$

where N is the total number of poles in the cluster. We initially planned on using $\hat{s}_\alpha$ as a final estimate of s_α. For low order, say $\alpha = 1,2$, the results are adequate. But the higher order poles had enough error that we looked for a way to improve the estimate. The problem with using $\hat{s}_\alpha$ as an estimate is that the $\hat{s}_\alpha(\theta,z)$ are biased estimates of s_α. Averaging tends to remove the random component of error but can do nothing about the bias. It would be better if some of the noise could be averaged out of the original data records before calculation of the pole estimates. This suggests averaging the data records instead of the $\hat{s}_\alpha(\theta,z)$. The data

records used in the averaging ought to be those where the α-natural mode is near a peak. That is, the average should be weighted approximately in proportion to the natural mode.

As a next step we used the $\hat{s}_\alpha$ as poles and computed residue estimates $\hat{R}_\alpha(\theta,z)$ from the data. For the value of $\theta = \theta_o$ that appeared to give the largest range of variation in the magnitude of $\hat{R}_\alpha(\theta,z)$ we computed an estimate of the normalized natural mode $\hat{i}_\alpha(\theta_o,z)$. This natural mode is an estimate of which data records have the best signal to noise ratio for the α-natural frequency component. The data $y(t,\theta_o,z)$ corresponding to z values where $\hat{i}_\alpha(\theta_o,z)$ is approximately ± 1 should be the best data for estimating s_α. Let

$$\hat{\Phi}_\alpha(t) = \sum_z W_\alpha(z) y(t,\theta_o,z) \qquad (19)$$

be a weighted average of the data. ($\hat{\Phi}_\alpha(t)$ depends on θ_o but we will not explicitly show this.) The sum is taken over the available z values. One choice for the weight function $W_\alpha(z)$ is to make it proportional to the estimated natural mode $\hat{i}_\alpha(\theta_o,z)$. This proved to be an acceptable choice for low values of α since the corresponding $\hat{i}_\alpha(\theta_o,z)$ is fairly smooth. But with $\alpha = 5$, for example, the natural mode estimate is more erratic. As a result we used a coarse weight function that was proportional to +1 for z values that make $\hat{i}_\alpha(\theta_o,z) \simeq 1$, equal to -1 for z values that make $\hat{i}_\alpha(\theta_o,z) \simeq -1$ and equal to zero otherwise. Figures 25, 26, and 27 show graphs of the $\hat{\Phi}_\alpha(t)$ obtained for $\alpha = 1$, 3, and 5. The

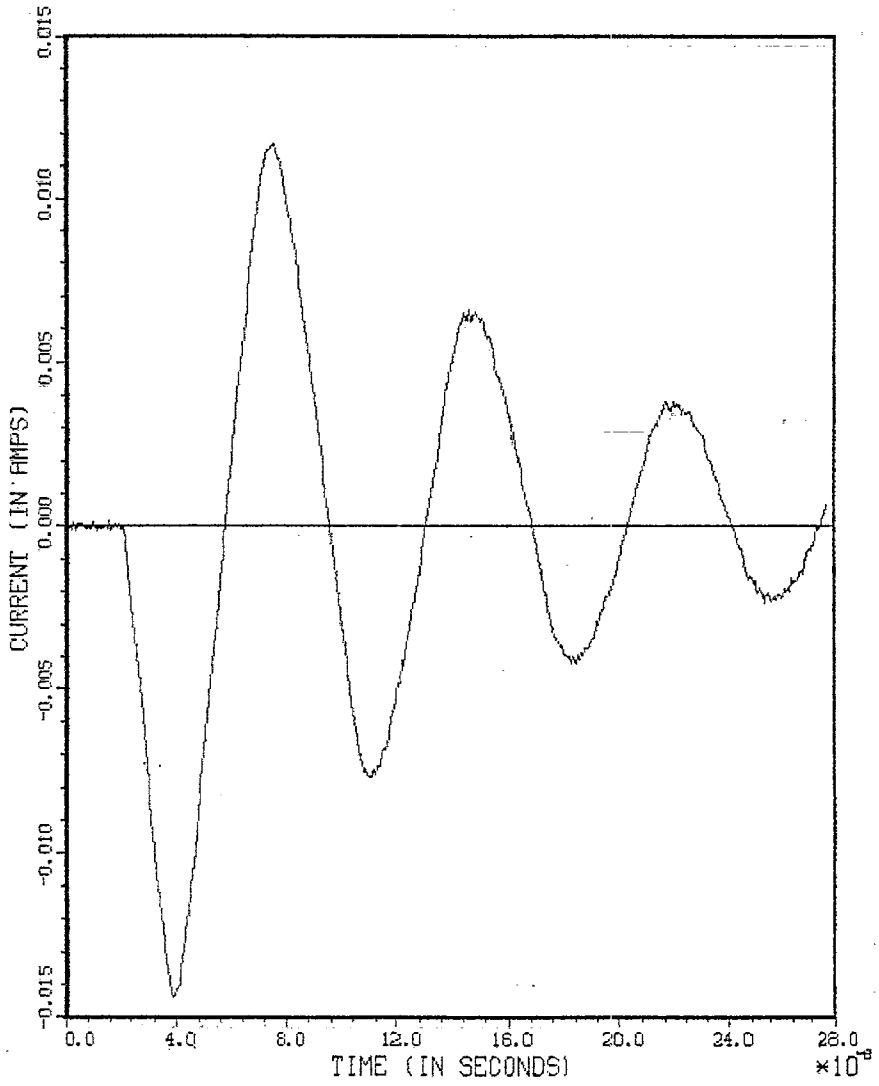

Figure 25. $\hat{\Phi}_{\alpha}(t)$ for $\alpha = 1$

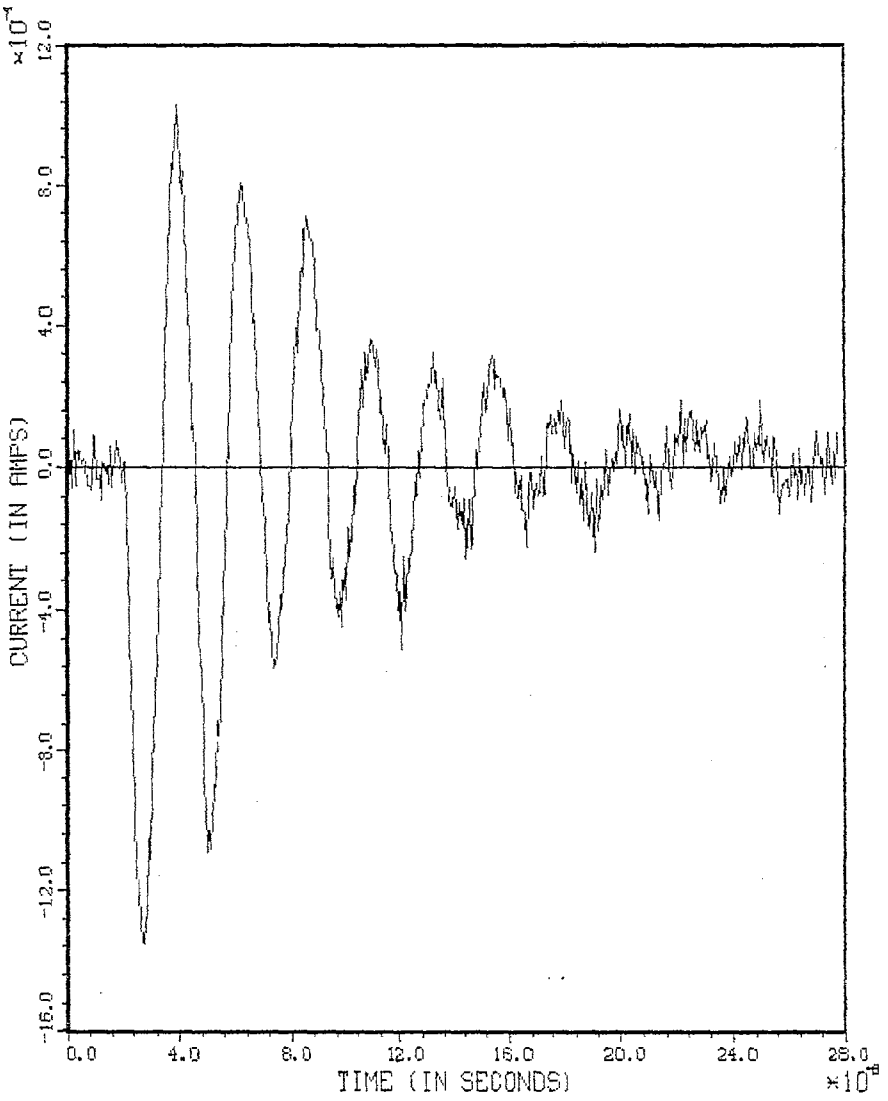

Figure 26. $\hat{\Phi}_{\alpha}(t)$ for $\alpha = 3$

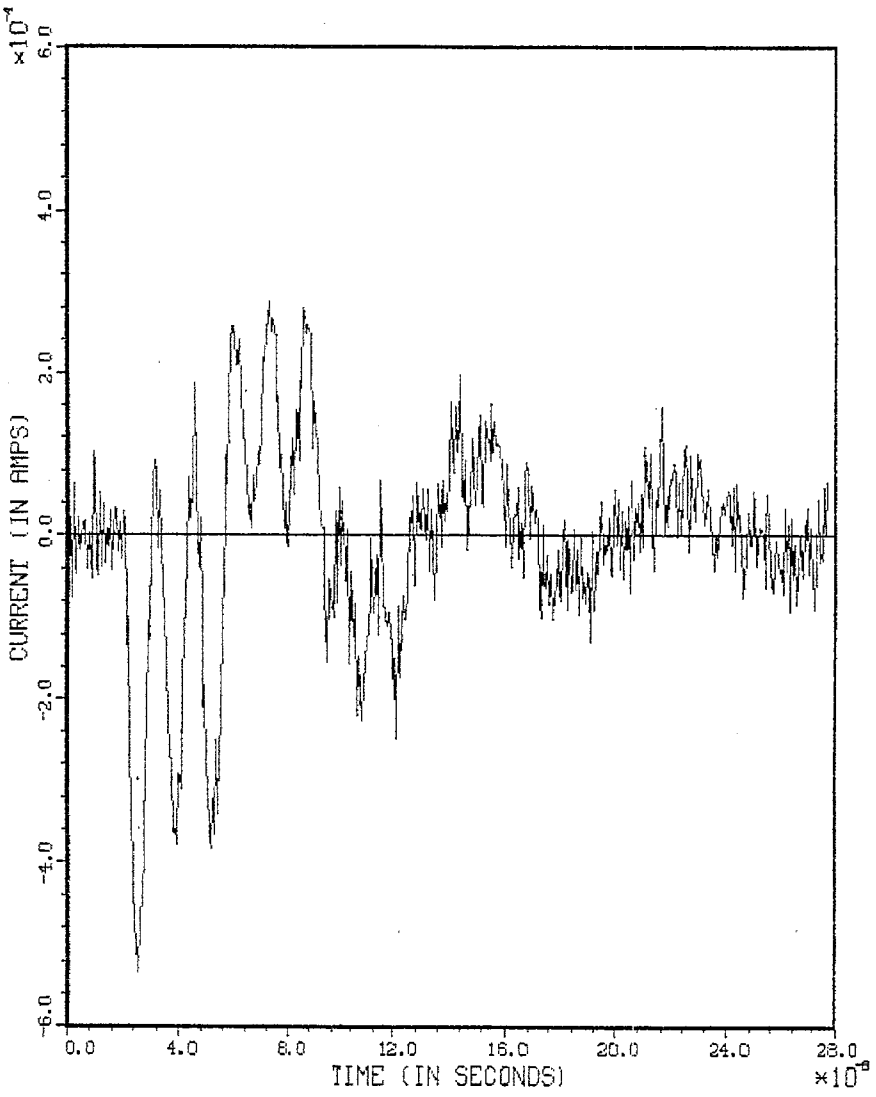

Figure 27. $\hat{\phi}_{\alpha}(t)$ for $\alpha = 5$

weight functions $W_\alpha(z)$ were chosen to average six, nine, and fifteen data records, respectively. The graphs indicate that the noise level increases as α goes from 1 to 5.

The pole estimate $\bar{s}_\alpha$ computed from $\hat{\Phi}_\alpha(t)$ should be better than from an estimate computed from any one of the $y(t,\theta,z)$. This is because the noise variance is reduced by the average over z. Moreover, the pole estimate computed from $\hat{\Phi}_\alpha(t)$ should be better than an estimate computed from averaging the $\hat{s}_\alpha(\theta,z)$. This is because the $\hat{s}_\alpha(\theta,z)$ contains a bias error while the original data records $y(t,\theta,z)$ do not (according to our assumption about the noise having zero mean).

As an example of the results from using the $\hat{\Phi}_\alpha(t)$ technique with $\theta = 0°$, we have

$$\bar{s}_1 = -0.0824553 + j0.9183957$$

$$\bar{s}_3 = -0.1581486 + j2.879185$$

$$\bar{s}_5 = -0.1893679 + j4.834777$$

These pole estimates still have some error, of course, but they are better results than we were able to get by averaging the $\hat{s}_\alpha(\theta,z)$ values computed from the same data.

Figures 25, 26, and 27 show an interesting fact. The $\hat{\Phi}_\alpha(t)$ contain mostly the α natural frequency. To see why this is the case, consider neglecting $g(t,\theta,z)$ and rewriting Equation 3 as

$$I(t,\theta,z) = \sum_\alpha \Phi_\alpha(t) \sin(\alpha\pi z/L), \qquad 0 \leq z \leq L, \quad \alpha = 1,2,3,..... \qquad (20)$$

where

$$\Phi_\alpha(t) = 2\mathrm{Re}\left[\eta_\alpha^{\max}\eta_\alpha^{1}(\theta)\tilde{f}(s_\alpha)\,\exp(s_\alpha t)\right]u(t-t_o) \qquad (21)$$

and where the approximation of Equation 4 is used for the natural mode. Equation 20 has the form of a Fourier series in z.

The Fourier series coefficients $\Phi_\alpha(t)$ are given by

$$\Phi_\alpha(t) = \frac{2}{L}\int_0^L I(t,\theta,z)\,\sin(\alpha\pi z/L)dz \qquad (22)$$

The function $\Phi_\alpha(t)$ contains time behavior corresponding to s_α alone. If the integral in Equation 22 is approximated by a sum over M values of z spaced Δz apart, then we can write

$$\Phi_\alpha(t) \simeq \frac{2\Delta z}{L}\sum_{i=1}^{M} I(t,\theta,z_i)\,\sin(\alpha\pi z_i/L) \qquad (23)$$

where the z_i are the z values. This equation compares with Equation 19. The functions $\Phi_\alpha(t)$ establish a bound on how well the various natural frequencies can be separated.

The $\Phi_\alpha(t)$ were computed from noisy data and the results are plotted in Figures 28, 29, and 30 for α = 1, 3, and 5. In these calculations M = 60 and Δz = 10/60 meter. The pole values $\tilde{s}_\alpha$ estimated from applying the iterative prefilter algorithm to $\Phi_\alpha(t)$ are

$$\tilde{s}_1 = -0.08219866 + j0.9187515$$

$$\tilde{s}_3 = -0.1480808 + j2.877230$$

$$\tilde{s}_5 = -0.1933258 + j4.847712$$

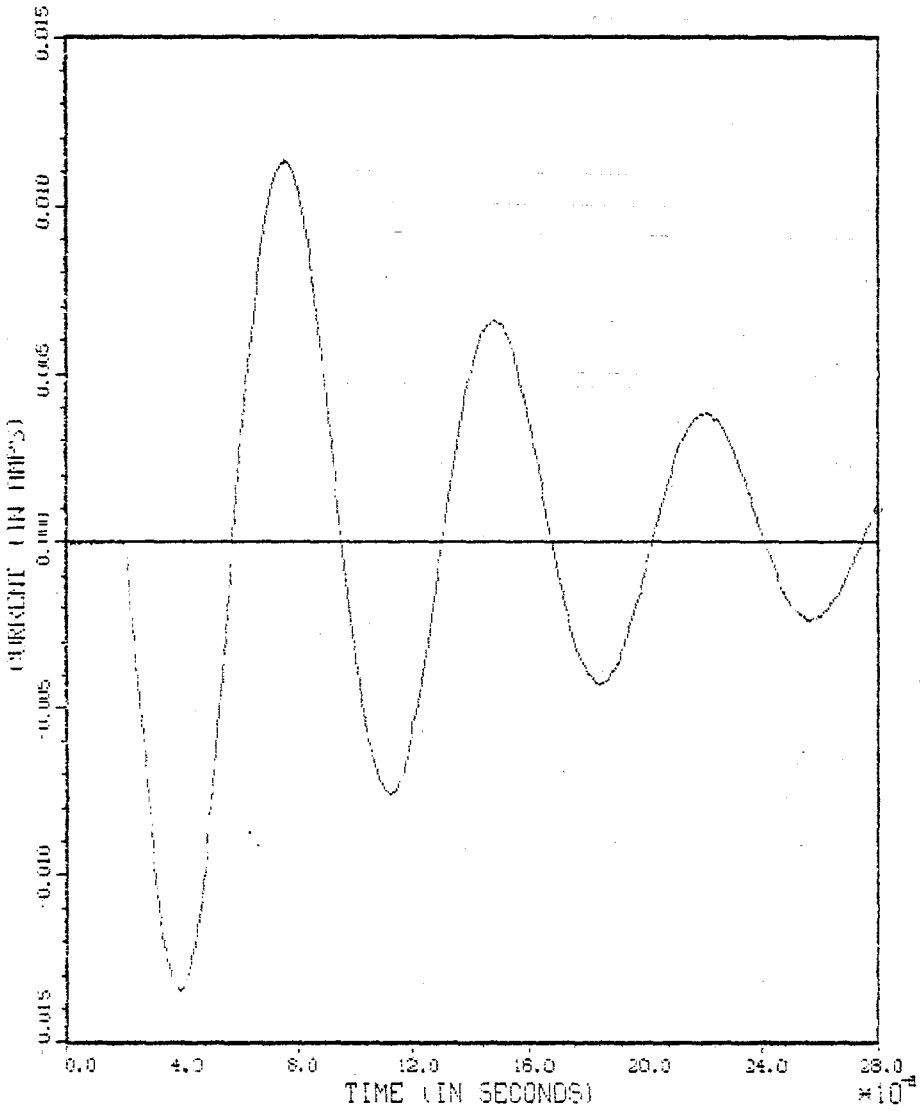

Figure 28. Plot of $\Phi_\alpha(t)$ for $\alpha = 1$

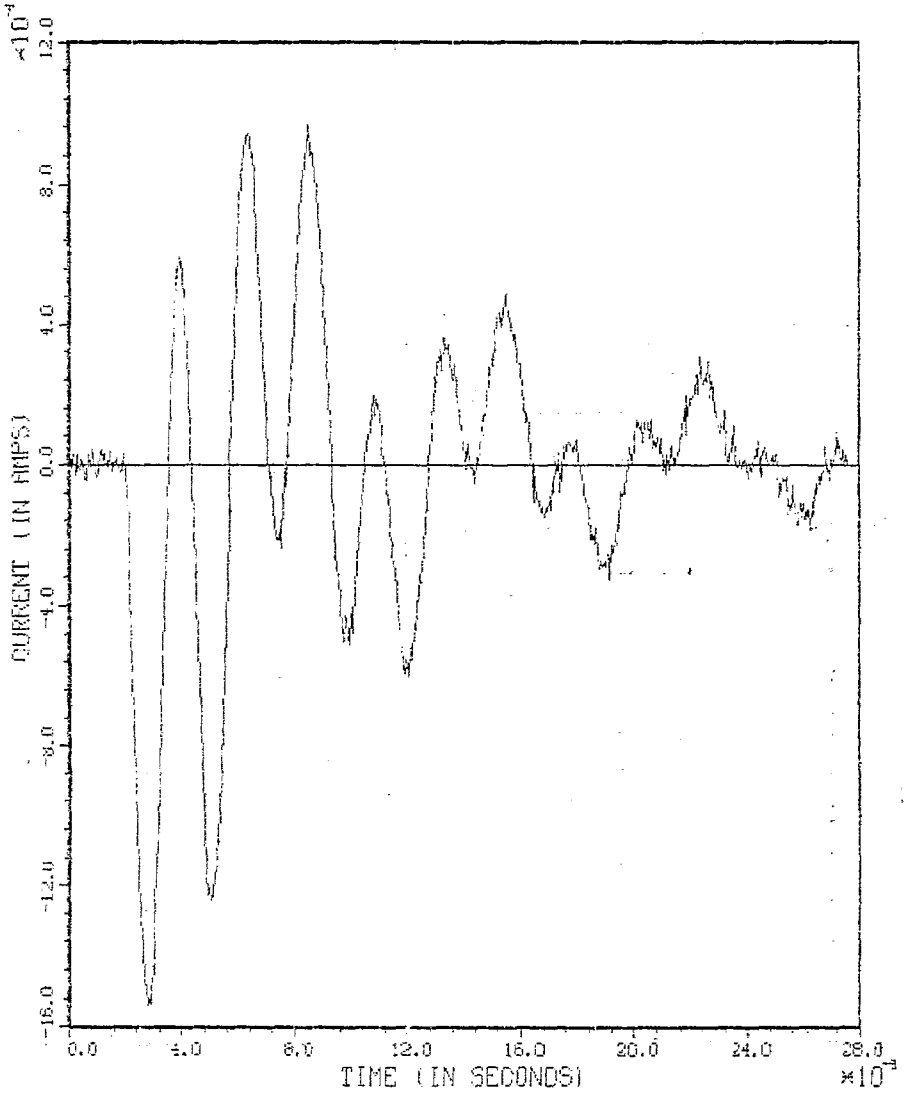

Figure 29. Plot of $\Phi_\alpha(t)$ for $\alpha = 3$

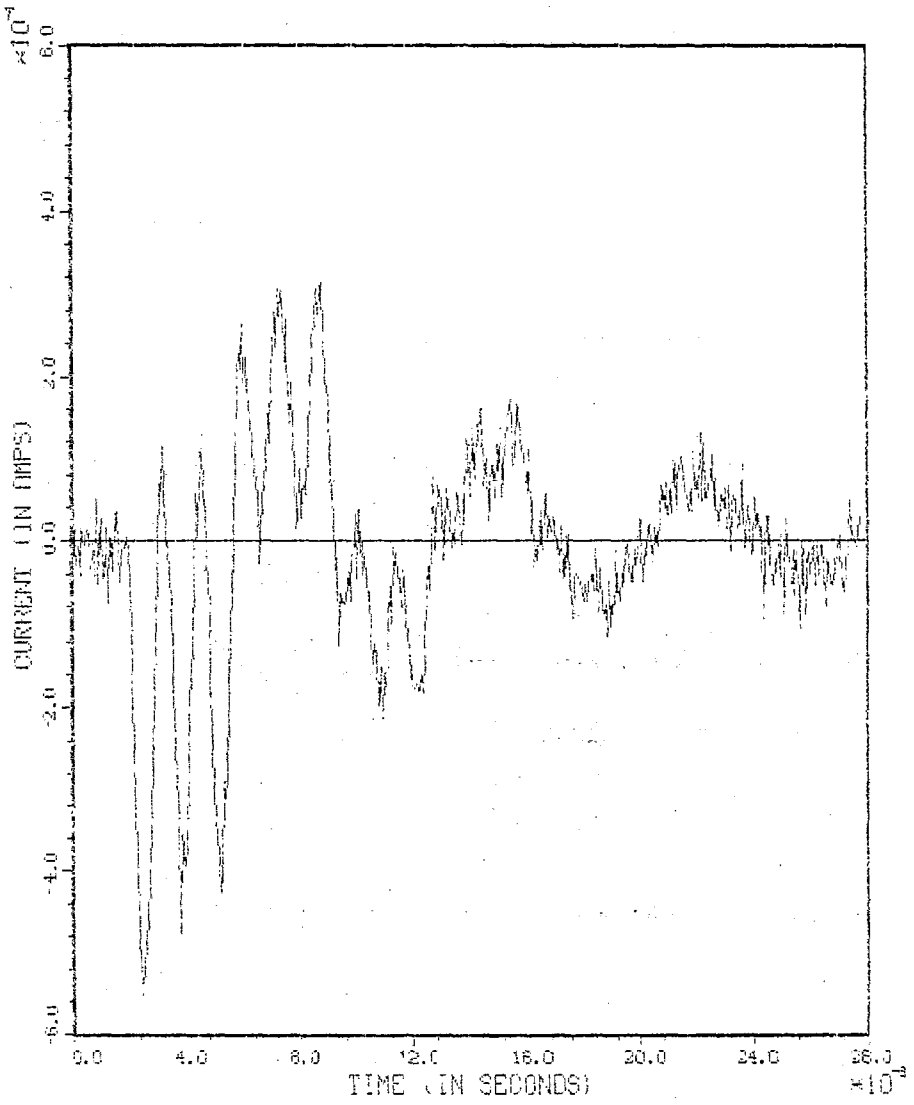

Figure 30. Plot of $\Phi_\alpha(t)$ for $\alpha = 5$

As would be expected, these results are better than those obtained from the $\hat{\Phi}_\alpha(t)$. Unfortunately, the procedure is not practical since we usually do not know the natural modes. And of course the modes are not exactly orthogonal. The thin wire is a special case in that the modes are approximately orthogonal. But the principle is that the data should be weighed proportionally to the natural modes.

The technique for calculation of $\hat{\Phi}_\alpha(t)$ could be extended by averaging several $\hat{\Phi}_\alpha(t)$ functions computed with different θ values--perhaps weighed by an estimate of the coupling coefficient. This was not tried.

From the form of Equation 2, it is clear that for some values of θ and z not all the modes are present in $I(t,\theta,z)$. This is simply because of zeros in $n_\alpha^1(\theta)$ and $i_\alpha(z)$. When the data are noisy, there is a "dead zone" around the zeros of these functions where the signal to noise ratio is low, and the natural frequencies cannot be estimated accurately. For experimental data we expect that it may be necessary to use a two step measurement approach. At the first step one places sensors of the test object guided by some pretest calculations. After analyzing the resulting data and estimating the SEM parameters, the second step is to modify the sensor placement and field orientation to better identify some modes or to find missing modes.

3.2.3 The Effect of Noise on the Natural Modes

In order to prevent the occurrence of bias error resulting from the pole estimation process, the best pole values obtained should be used to compute the residues for the determination of the natural modes. If the pole values are accurately known, then approximately unbiased solutions for residues will be obtained.

The real and imaginary parts of the natural modes calculated by using the pole values obtained from both $\hat{\Phi}_\alpha(t)$ and $\Phi_\alpha(t)$ are presented in Figures 31 through 34 for $\alpha = 1$, 3, and 5. The graphs indicate that noise is more of a problem with the higher frequency modes than with the fundamental.

The results obtained can be improved by averaging the natural modes for the same α, computed from several values of θ. That is, one can compute estimates $\hat{i}_\alpha(\theta,z)$ of $i_\alpha(z)$ by using residues calculated from data obtained at different angles of incidence. Then an estimate of the natural mode is obtained as

$$\hat{i}_\alpha(z) = \frac{1}{N_\theta} \sum_\theta \hat{i}_\alpha(\theta,z) \qquad (24)$$

where N_θ is the number of different θ values used. This estimate is unbiased if the residue estimates are unbiased. And of course averaging reduces the error variance. The average could include a weight factor proportional to the coupling coefficient but this was not done.

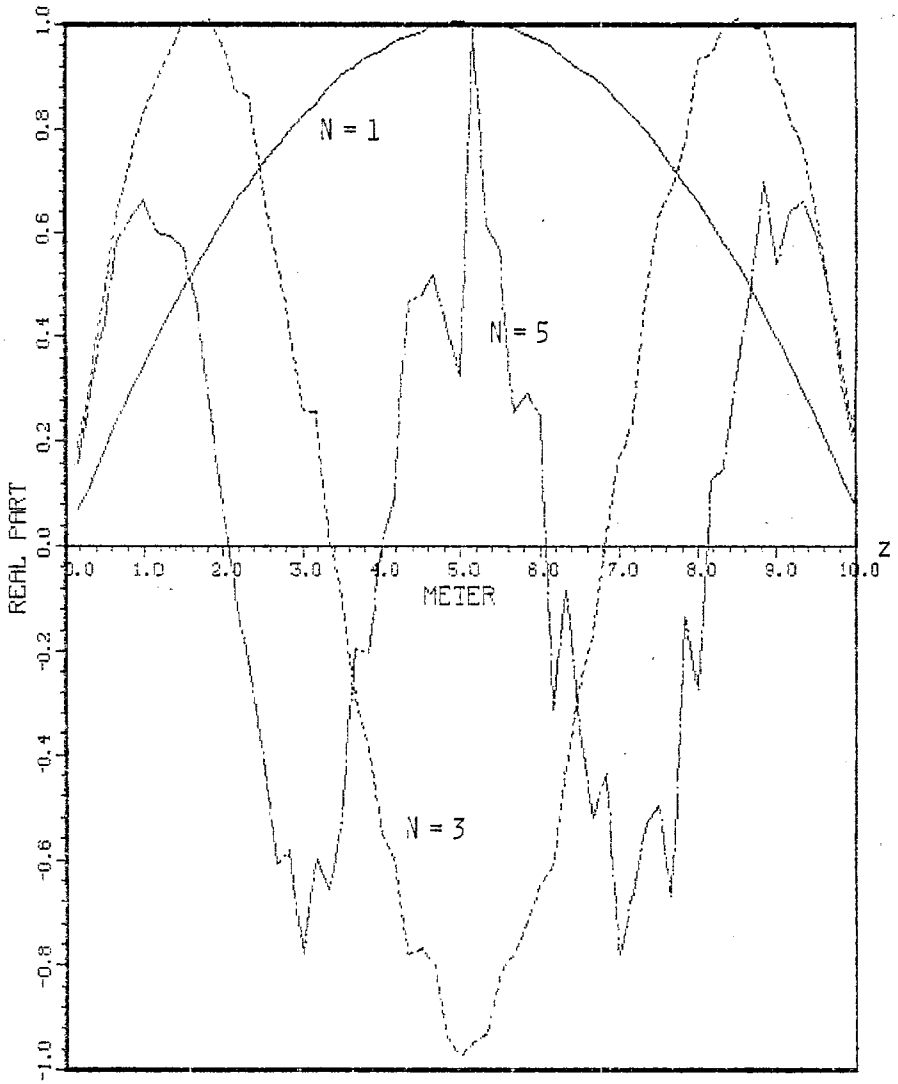

Figure 31. Real parts of normalized natural modes for α = 1,3,5, obtained from $\hat{\Phi}_{\alpha}(t)$

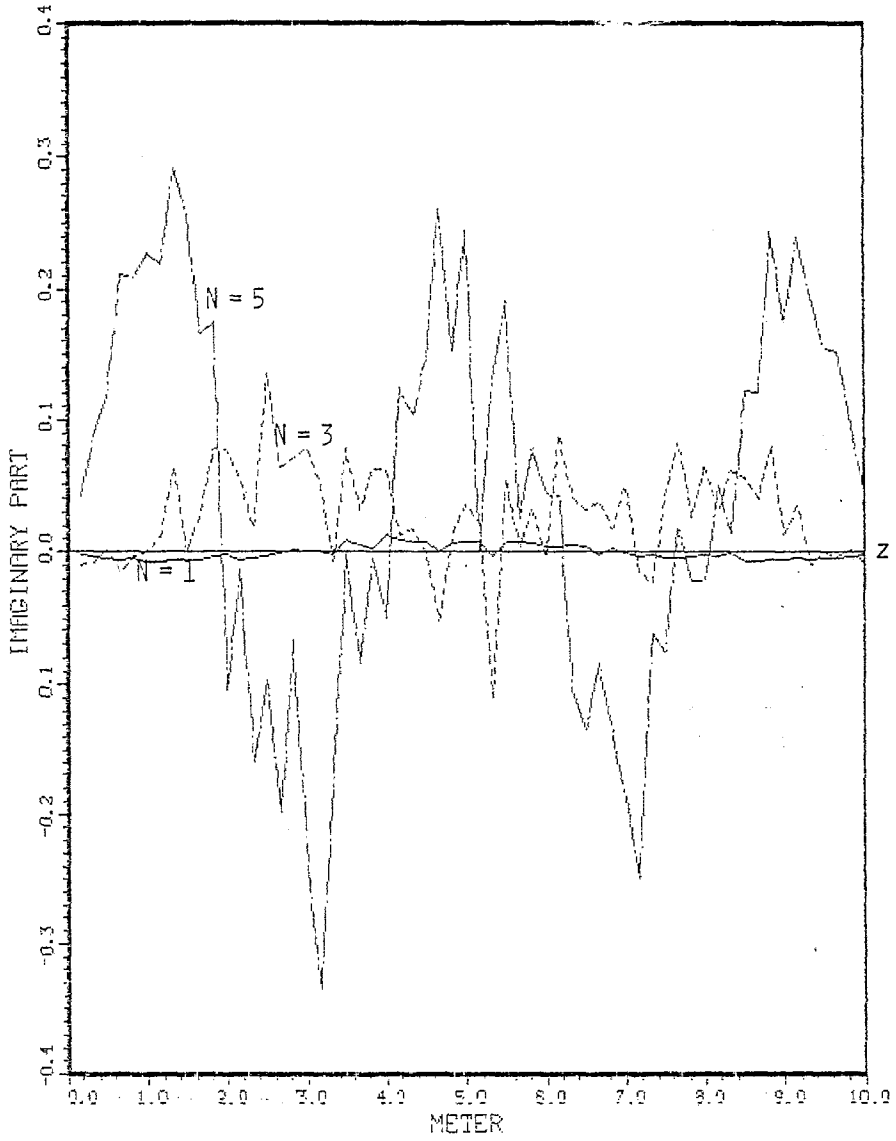

Figure 32. Imaginary parts of normalized natural modes for α = 1,3,5, obtained from $\hat{\Phi}_{\alpha}(t)$

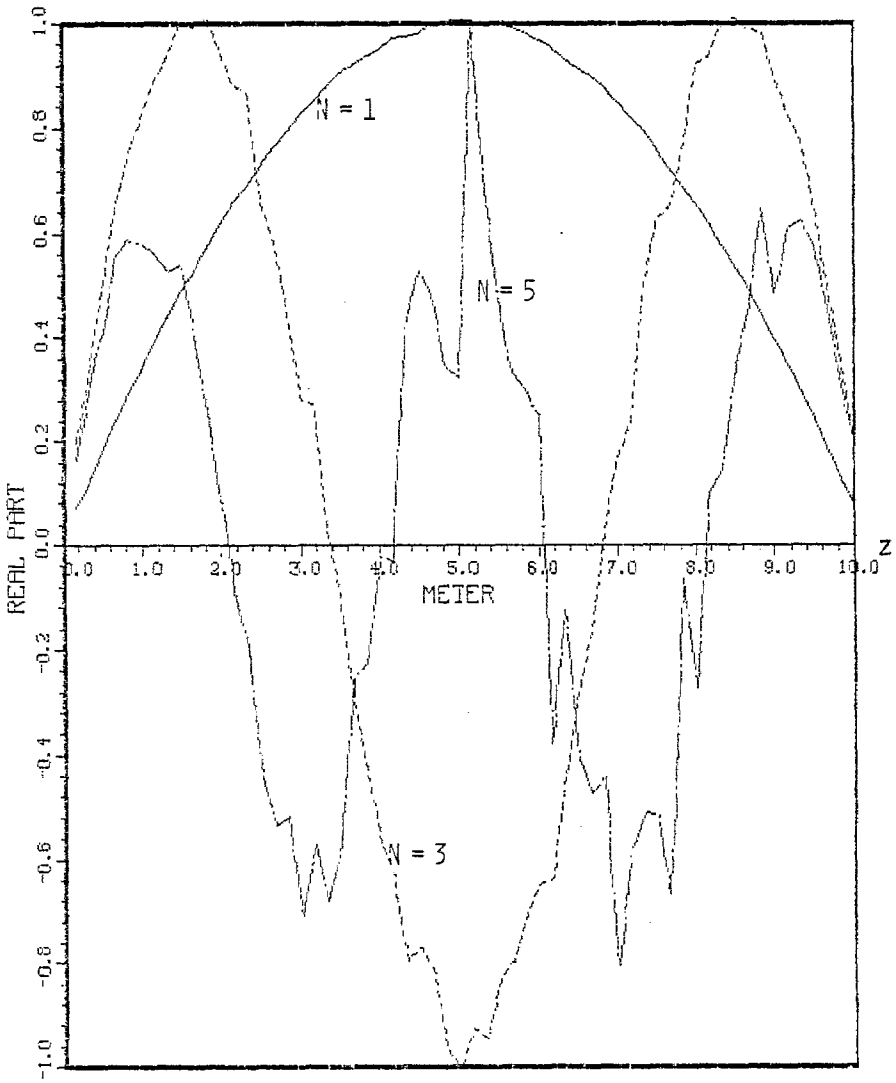

Figure 33. Real parts of normalized natural modes for α = 1,3,5, obtained from $\Phi_\alpha(t)$

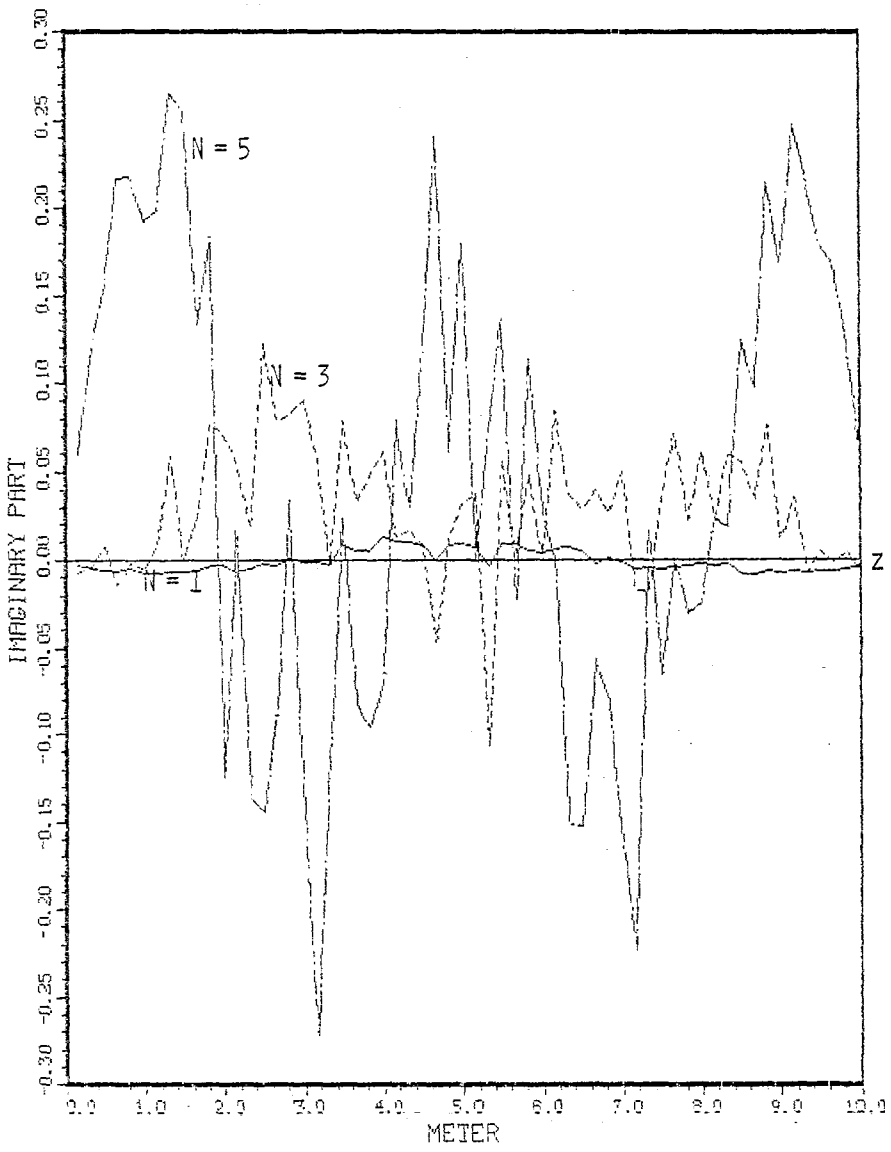

Figure 34. Imaginary parts of normalized natural modes for α = 1,3,5, obtained from $\Phi_\alpha(t)$

The averaged natural mode for $\alpha = 3$ is shown in Figures 35 and 36 for real and imaginary parts, respectively. Three uncorrelated noisy third modes were averaged to produce this result.

3.2.4 The Effect of Noise on the Coupling Coefficients

The coupling coefficients were computed by using the poles obtained from $\hat{\Phi}_\alpha(t)$ for the reason given in the previous section. The real and imaginary parts of the coupling coefficients for $\alpha = 1$, 2, and 3 are plotted in Figures 37 and 38, respectively. The coupling coefficient for $\alpha = 3$ was improved by averaging three noisy third modes. The average has the form

$$\hat{\eta}_\alpha^1(\theta) = \frac{1}{N_z} \sum_z \hat{\eta}_\alpha^1(\theta,z) \qquad (25)$$

where $\hat{\eta}_\alpha^1(\theta,z)$ is the normalized coupling coefficient at location z, and N_z is the number of z values used.

These results are presented in Figure 39, the real part; and Figure 40, the imaginary part.

3.2.5 The Effect of Noise on the Normalization Factors

The normalization factors can still be determined by Equation 16 since both the natural modes and coupling coefficients are now known. However, experience shows that because of residue error, a more accurate value will be achieved by averaging several η_α^{max} for the same α, which have been calculated from different values of θ and z. Averaging three noisy factors for each

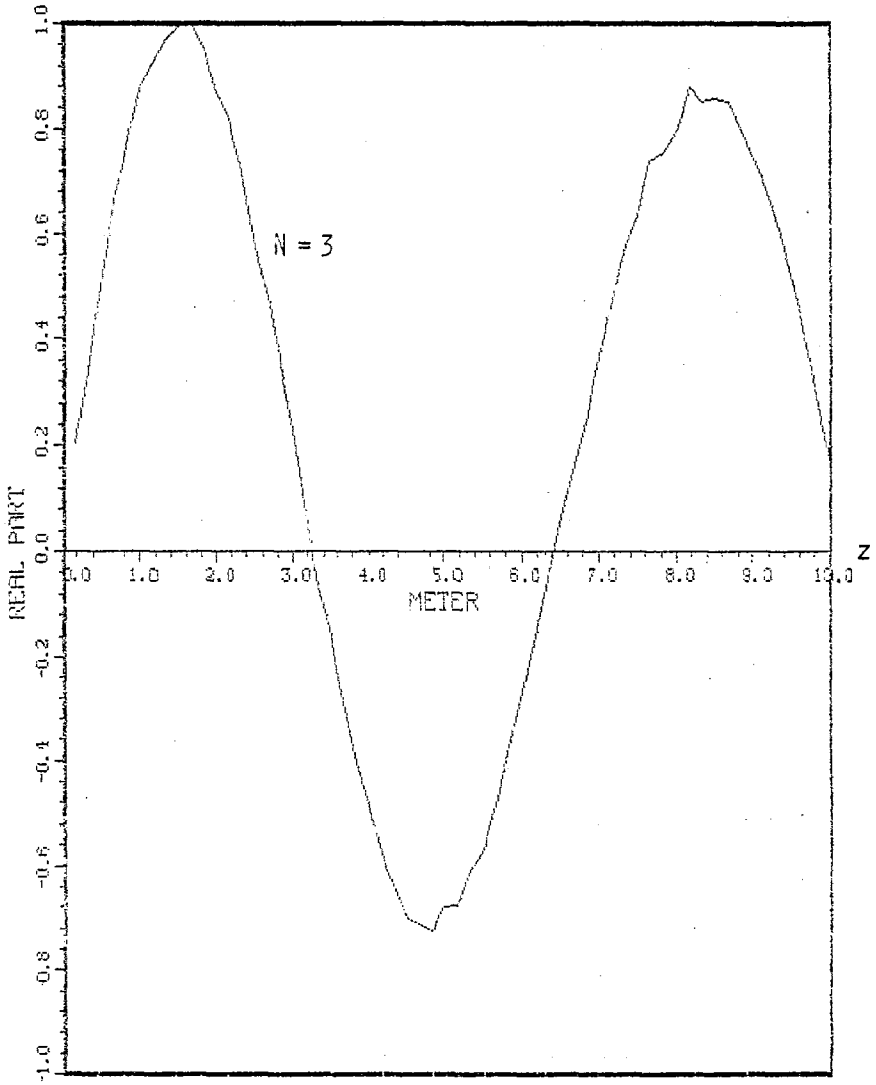

Figure 35. Real part of normalized natural modes for $\alpha = 3$, obtained by signal averaging

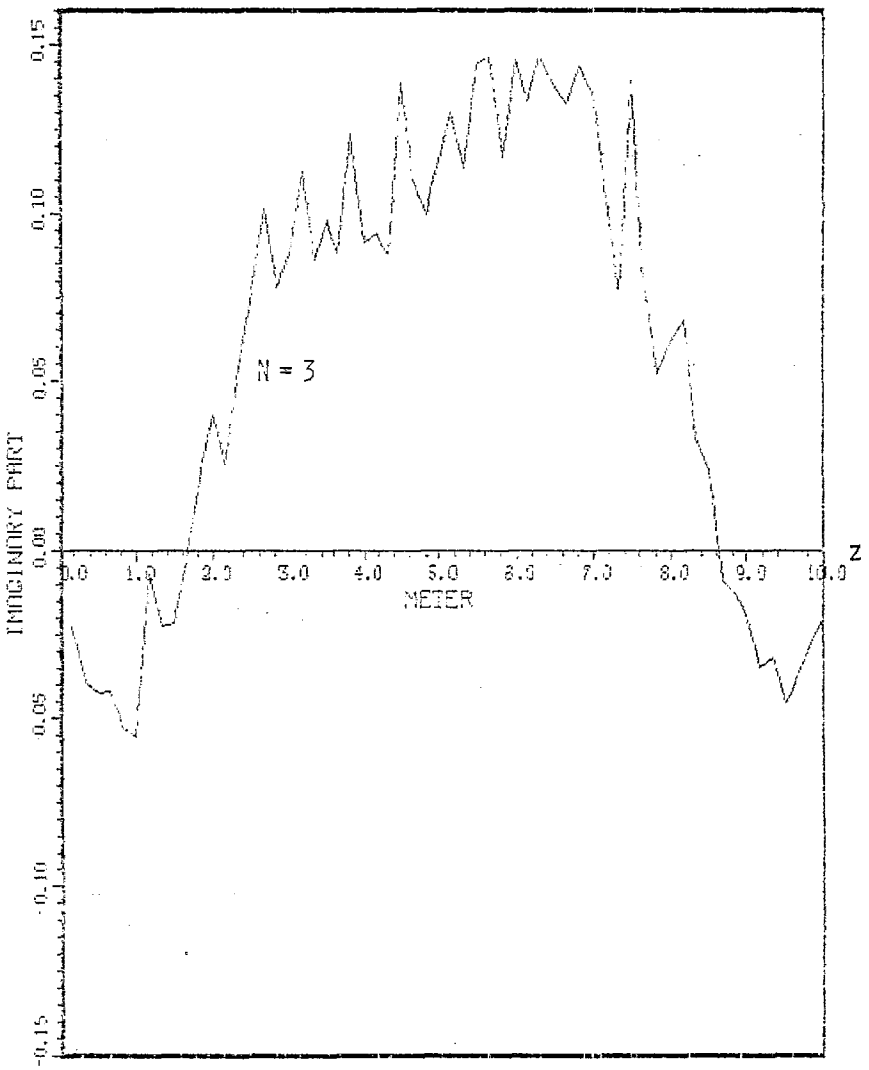

Figure 36. Imaginary part of normalized natural modes for α = 3, obtained by signal averaging

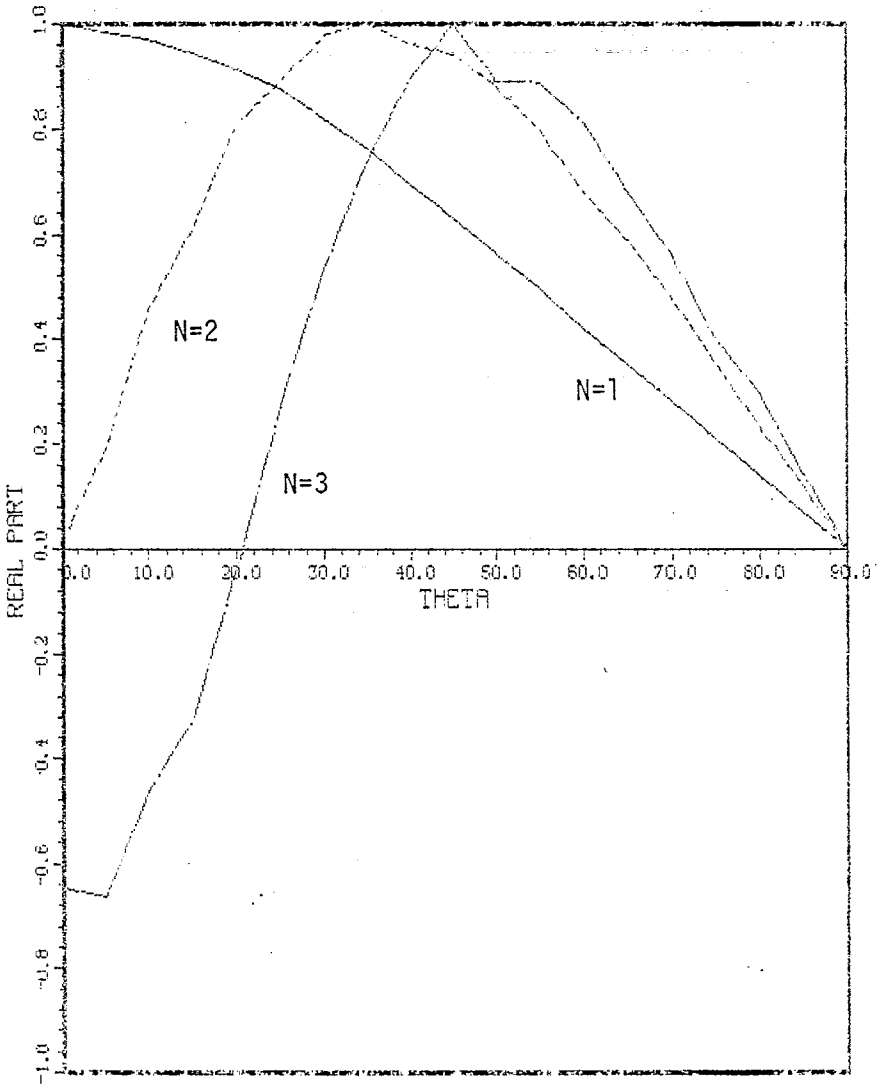

Figure 37. Real parts of normalized coupling coefficients for $\alpha = 1,2,3$, computed from $\hat{\Phi}_\alpha(t)$

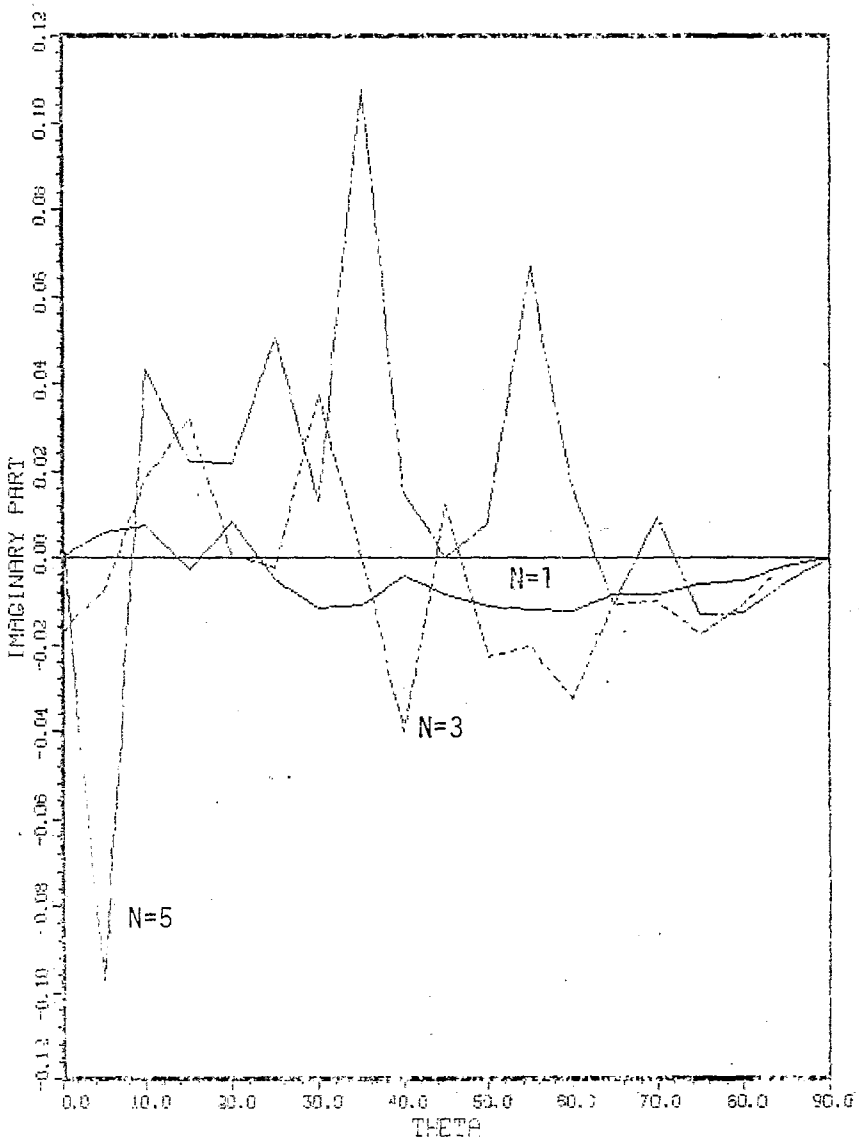

Figure 38. Imaginary parts of normalized coupling coefficients for $\alpha = 1,2,3$, computed from $\hat{\Phi}_{\alpha}(t)$

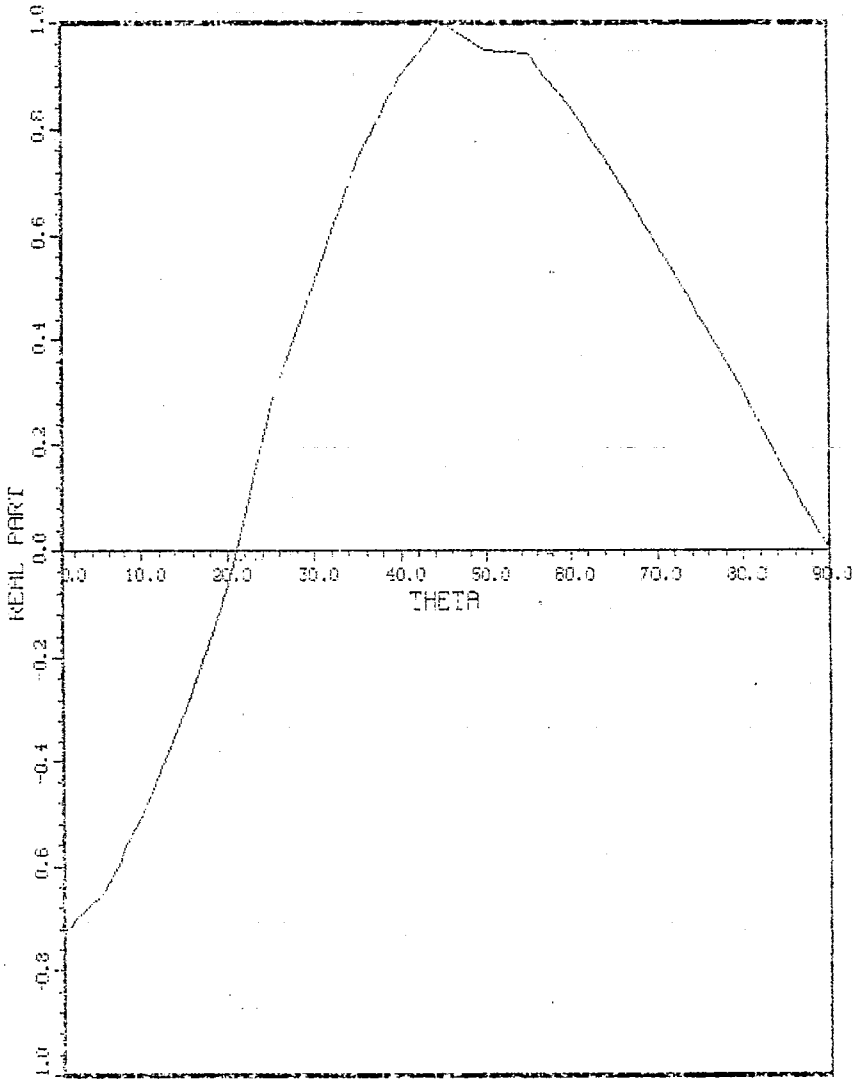

Figure 39. Real part of normalized coupling coefficients for $\alpha = 3$, obtained by signal averaging

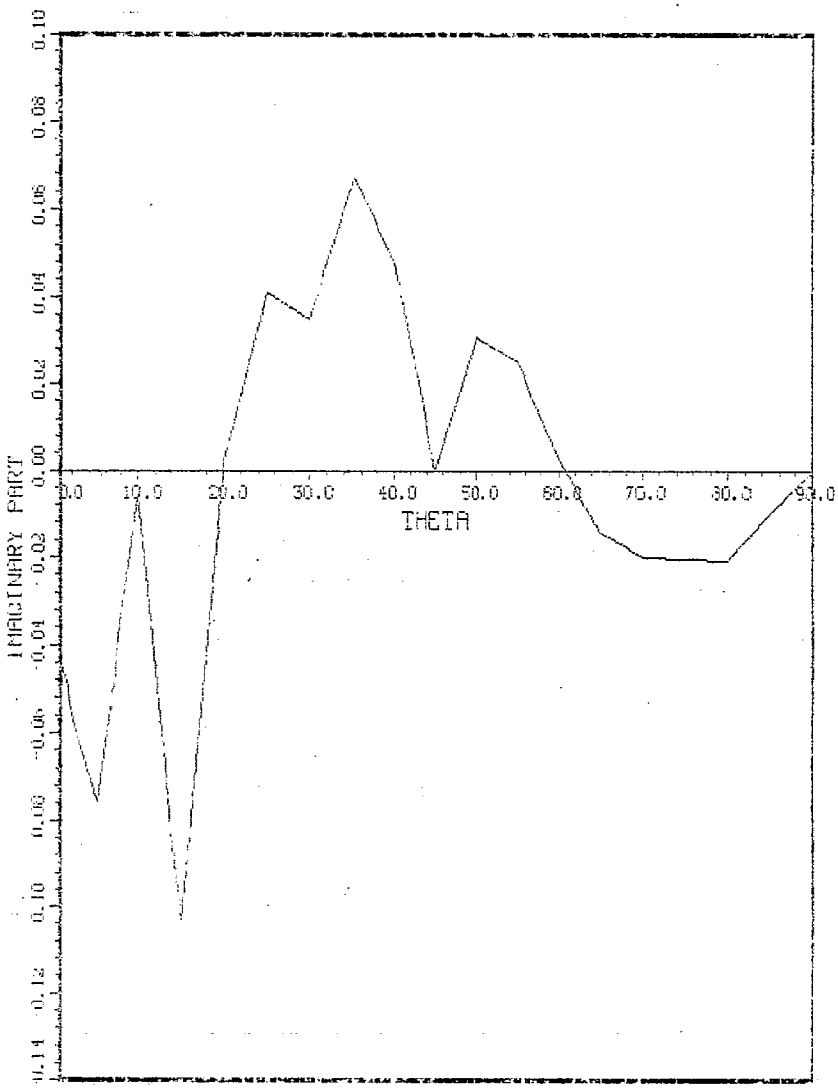

Figure 40. Imaginary part of normalized coupling coefficients for α = 3, obtained by signal averaging

case, we obtained the normalization factors for the first three resonant frequencies as

$$\eta_1^{max} = -0.7148283\times10^6 - j0.1935363\times10^6$$

$$\eta_2^{max} = 0.1383078\times10^6 - j0.4762430\times10^6$$

$$\eta_3^{max} = 0.4027178\times10^6 + j0.1609751\times10^6$$

Implicit in the η_α^{max} calculation is the assumption that $\tilde{f}(s_\alpha)$ is known exactly. This assumption is unrealistic for the higher frequency poles. In EMP testing, information on f(t) is obtained from field map data. From this data we can expect to estimate the low frequency behavior of $\tilde{f}(s)$ fairly well but not the high frequency behavior. So how accurately $\tilde{f}(s_\alpha)$ is known depends on s_α. For the low frequency poles of a large object, we expect only minor problems with the $\tilde{f}(s_\alpha)$ values.

CHAPTER IV

CONCLUSIONS

The SEM parameters for a thin wire can be evaluated directly from noiseless transient data using Prony's method. Our results agree well with Tesche's [3]. With noisy data, the iterative prefilter method gives better results. Averaging techniques can be used to enhance the values of the parameters. We tested two ways to improve the pole values. The first approach works simply by averaging several pole values for the same α which have been computed from the currents at different locations on the wire and different field orientations. This algorithm gave reasonably good results for the lower frequency poles. The second approach involves averaging several data records which have been weighed approximately in proportion to the natural modes. The poles can be extracted directly from these averages. This second technique gives more accurate pole values than the first.

It is interesting to note that only layer one poles [3] were found. The number of these poles needed to reconstruct the natural response of a thin-wire scatterer depends on the values of the natural modes, coupling coefficients, and incident field spectrum. For some responses, a two pole-pair reconstruction is adequate; other responses require ten or more pole pairs.

The best pole values should be used in the determination of the natural modes and coupling coefficients to minimize the effect of bias error. Then these parameter estimates can be improved by signal averaging. The values of the corresponding normalization factors can be improved by the same process. When these techniques are applied to an arbitrary test object, it may be necessary to use a two (or more) step process. At the first step sensor placement and incident field orientation are chosen based on pretest calculations and scale model results. After estimating the SEM parameters from the resulting data, the second step is to modify the sensor placement and field orientation to better identify some modes or to find missing modes.

The next phase of our research will be to treat more complicated structures which provide a better approximation to aircraft configurations. Our ultimate goal will be to see how the calculations are affected when coping with actual aircraft test data.

REFERENCES

[1] C. E. Baum, "The Singularity Expansion Method," Transient Electromagnetic Fields, edited by L. B. Felson. Springer-Verlag, 1976.

[2] C. E. Baum, "On the Singularity Expansion Method for the Solution of Electromagnetic Interaction Problems," Interaction Note 88. Air Force Weapons Laboratory, Kirtland Air Force Base, NM, December 1971.

[3] F. M. Tesche, "On the Singularity Expansion Method as Applied to Electromagnetic Scattering from Thin-Wires," Interaction Note 102. Air Force Weapons Laboratory, Kirtland Air Force Base, NM, April 1972.

[4] D. R. Wilton and K. R. Umashankar, "Parametric Study of an L-Shaped Wire Using the Singularity Expansion Method," Interaction Note 152. Air Force Weapons Laboratory, Kirtland Air Force Base, NM, November 1973.

[5] L. Marin, "Natural Modes of Certain Thin-Wire Structures," Interaction Note 186. Air Force Weapons Laboratory, Kirtland Air Force Base, NM, August 1974.

[6] L. Marin and T. K. Liu, "A Simple Way of Solving Transient Thin-Wire Problems," Interaction Note 253. Air Force Weapons Laboratory, Kirtland Air Force Base, NM, October 1975.

[7] M. L. Van Blaricum and R. Mittra, "A Technique for Extracting the Poles and Residues of a System Directly from Its Transient Response," Interaction Note 245. Air Force Weapons Laboratory, Kirtland Air Force Base, NM, February 1975.

[8] F. B. Hildebrand, Introduction to Numerical Analysis. McGraw-Hill, 1956.

[9] D. L. Lager, H. G. Hudson, and A. J. Poggio, User's Manual for SEMPEX: A Computer Code for Extracting Complex Exponentials from a Time Waveform. Lawrence Livermore Laboratory, CA, March 1977.

[10] H. G. Hudson and D. L. Lager, Observations on the Operation of the SEMPEX Code. Lawrence Livermore Laboratory, CA, September 1976.

[11] D. G. Dudley, "Fitting Noisy Data with a Compex Exponential Series," Mathematics Note 51. Air Force Weapons Laboratory, Kirtland Air Force Base, NM, March 1977.

[12] J. T. Cordaro, "Pole Measurements for the ATHAMAS Pipe Test," Mathematics Note 56. Air Force Weapons Laboratory, Kirtland Air Force Base, NM, August 1977.

[13] L. W. Pearson and D. R. Robertson, "Extrapolation of Induced Transient Surface Currents on a Scatterer to a General Band-Limited Excitation Conditions," Interaction Note 360. Air Force Weapons Laboratory, Kirtland Air Force Base, NM, October 1978.

[14] K. Steiglitz and L. E. McBride, "A Technique for the Identification of Linear System," IEEE Transaction on Automatic Control, Vol. AC-10, October 1965.

[15] L. D. Scott, "Deterministic Error Analysis Applied to EMP Simulator Data Acquisition," Measurement Note 24. Air Force Weapons Laboratory, Kirtland Air Force Base, NM, June 1977.

[16] G. M. Jenkins and D. G. Watts, Spectral Analysis and Its Application. Holden-Day, 1968.

[17] J. A. Landt, E. K. Miller, and M. L. Van Blaricum, "A Computer Program for the Time-Domain Electromagnetic Response of Thin-Wire Structures," Interaction Note 210. Air Force Weapons Laboratory, Kirtland Air Force Base, NM, May 1974.

[18] B. K. Singaraju, D. V. Giri and C. E. Baum, "Further Developments in the Application of Contour Integration to the Evaluation of the Zeros of Analytic Functions and Relevant Computer Programs," Mathematics Note 42. Air Force Weapons Laboratory, Kirtland Air Force Base, NM, March 1976.